

# Co-optimization for Adaptive Conformal Prediction

Xiaoyi Su<sup>\*1</sup>, Zhixin Zhou<sup>†2</sup>, and Rui Luo<sup>‡1</sup>

<sup>1</sup>Department of Systems Engineering, City University of Hong Kong, Hong Kong SAR, China

<sup>2</sup>Alpha Benito Research, Los Angeles, USA

## Abstract

Conformal prediction (CP) provides finite-sample, distribution-free marginal coverage, but standard conformal regression intervals can be inefficient under heteroscedasticity and skewness. In particular, popular constructions such as conformalized quantile regression (CQR) often inherit a fixed notion of center and enforce equal-tailed errors, which can displace the interval away from high-density regions and produce unnecessarily wide sets. We propose **Co-optimization for Adaptive Conformal Prediction (CoCP)**, a framework that learns prediction intervals by jointly optimizing a center  $m(x)$  and a radius  $h(x)$ . CoCP alternates between (i) learning  $h(x)$  via quantile regression on the folded absolute residual around the current center, and (ii) refining  $m(x)$  with a differentiable soft-coverage objective whose gradients concentrate near the current boundaries, effectively correcting mis-centering without estimating the full conditional density. Finite-sample marginal validity is guaranteed by split-conformal calibration with a normalized nonconformity score. Theory characterizes the population fixed point of the soft objective and shows that, under standard regularity conditions, CoCP asymptotically approaches the length-minimizing conditional interval at the target coverage level as the estimation error and smoothing vanish. Experiments on synthetic and real benchmarks demonstrate that CoCP yields consistently shorter intervals and achieves state-of-the-art conditional-coverage diagnostics.

## 1 Introduction

Even though conformal prediction (CP) [43, 39, 29, 1] provides a flexible and distribution-free recipe for constructing prediction sets with finite-sample *marginal* coverage under exchangeability, high-quality prediction intervals must do more than simply meet a nominal coverage level. They should be *as short as the conditional distribution permits* while adapting to heteroscedasticity and shape changes across the covariate space. In this context, Conformalized Quantile Regression (CQR) [35, 37] has emerged as a particularly popular and effective instantiation, combining conditional quantile estimation with conformal calibration to produce heteroscedastic, marginally valid prediction intervals.

For comparison against the theoretical minimum length, the ideal benchmark is the highest density interval (HDI). By the Neyman-Pearson lemma, the shortest region capturing  $1 - \alpha$  probability mass is exactly a density level set  $\{y : f(y) \geq \lambda\}$ , which under unimodality reduces to the contiguous HDI [6, 23]. For interior solutions, its endpoints naturally satisfy an equal-density boundary condition. However, standard methods like CQR enforce equal-tailed error rates (e.g.,  $\alpha/2$  on each side). Under skewed distributions, this rigid equal-tailed constraint systematically displaces the interval from high-density regions, yielding unnecessarily long intervals even when conditional coverage is perfectly maintained (Figure 1a). This contrast highlights the central challenge: to construct an optimally efficient  $(1 - \alpha)$ -interval, a method must not only *scale* to accommodate local noise but also *translate* its center toward the concentration of probability mass.

The core insight of this paper is a geometric pathway from any interval to an HDI-like interval, conceptualized via the “folded-flag” visualization in Figure 1. Consider an interval parameterized

---

\*xiaoyisu3-c@my.cityu.edu.hk

†zzhou@alphabenito.com

‡ruiluo@cityu.edu.hk

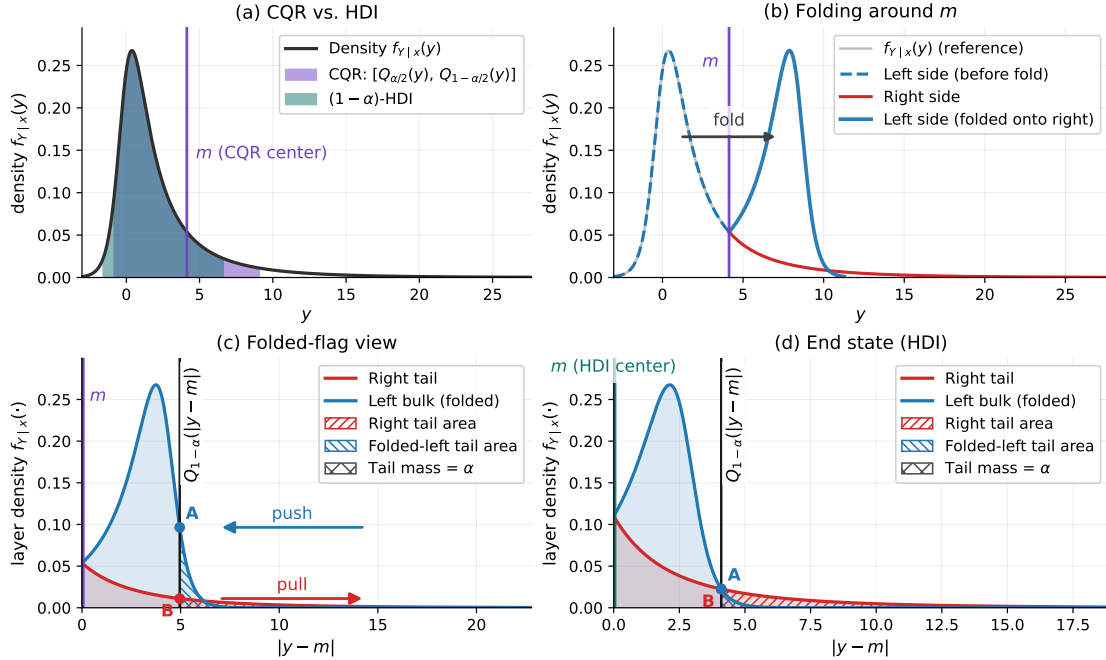


Figure 1: **From any interval to HDI via folding and boundary balancing.** (a) Under skewness, equal-tailed intervals can be displaced relative to the  $(1 - \alpha)$ -HDI and are typically longer. (b) Folding around a candidate center  $m$  maps  $y$  to  $|y - m|$ , producing a two-layer view. (c) The folded  $(1 - \alpha)$ -boundary corresponds to two endpoints; translating  $m$  shortens the interval when the endpoint densities are imbalanced (push–pull). (d) At equilibrium the endpoint densities match, recovering the HDI.

by a center  $m(x)$  and a radius  $h(x)$ . For a fixed center  $m$ , the radius required to capture  $1 - \alpha$  conditional mass is determined by a single boundary quantity: the  $(1 - \alpha)$ -quantile of the folded residual  $|Y - m(X)| \mid X = x$ . If the conditional densities at the two corresponding endpoints are imbalanced, translating  $m$  slightly toward the higher-density side shifts the data distribution relative to the center. Visually, this relative motion *pushes* denser probability mass into the interval while *pulling* sparser mass out (Figure 1c). Because a net positive mass enters the interval, the boundary quantile—and thus the radius  $h$ —must contract to maintain the exact  $1 - \alpha$  mass, thereby shortening the interval. This “push–pull” dynamic continues until the endpoint densities balance, which, under unimodality, perfectly recovers the HDI (Figure 1d). Thus, the discrepancy between any intervals and HDI-like intervals can be elegantly framed as a *boundary-balancing* problem in a folded geometry.

We operationalize this principle with **CoCP** (**Co**-optimization for adaptive **Co**nformal **P**rediction). CoCP explicitly couples the learning of  $m(x)$  and  $h(x)$ , enabling the interval to simultaneously translate and scale. Specifically,  $h$  tracks the folded  $(1 - \alpha)$ -boundary via a pinball loss, while  $m$  is refined using a differentiable *soft-coverage* surrogate. This surrogate cleverly concentrates the learning signal near the interval endpoints (Figure 2), directly capturing the boundary imbalance without requiring full conditional density estimation. Finally, we apply a standard conformal calibration step to guarantee exact finite-sample *marginal* coverage. In sum, our co-optimization stage determines the interval’s adaptive geometry to maximize efficiency and improves conditional reliability, while the calibration stage ensures rigorous validity. Our main contributions are summarized as follows:

- **HDI-motivated viewpoint and folded geometry.** We introduce a folded boundary-balancing perspective that explains the inefficiency of center-invariant conformal intervals under skewness. This motivates co-optimizing an interval center and radius to recover HDI-like translation and scaling.
- **A practical, co-optimized construction (CoCP).** We instantiate this perspective into a differentiable alternating optimization framework. Beyond guaranteeing finite-sample marginal validity, we theoretically establish that, under standard regularity conditions, CoCP asymptotically recovers the optimal conditional interval length and achieves exact conditional coverage as learning errors and the smoothing parameter vanish.

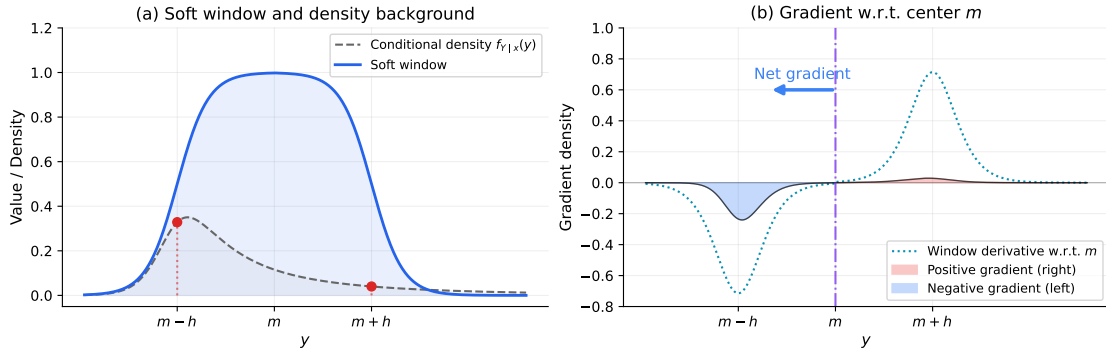


Figure 2: **Gradient dynamics of the soft-coverage objective.** (a) The soft window serves as a differentiable surrogate for the interval indicator. The underlying data density (dashed line) is imbalanced at the two boundaries. (b) The gradient of the soft window with respect to the center  $m$  acts as a signed sampling kernel, being negative at the left boundary and positive at the right. The resulting local gradient (the product of the conditional density and the derivative kernel) is asymmetric under skewness; the higher-density boundary generates a dominant directional signal that shifts the center  $m$  toward the concentration of probability mass.

- **Extensive empirical evidence.** We validate CoCP across diverse synthetic and real-world benchmarks, demonstrating that it not only yields significantly tighter intervals but also consistently achieves state-of-the-art conditional coverage diagnostics.

## 2 Related Work

Work on efficient conformal regression intervals often starts from CQR, which conformalizes estimated lower and upper conditional quantiles to obtain heteroscedastic but *equal-tailed* (typically  $\alpha/2$  and  $1 - \alpha/2$ ) intervals [35, 37]. A prominent alternative is *distributional* conformal inference [9, 24], which aims to better match skewed or multimodal conditionals by first learning richer conditional information and then extracting high-density sets. Conformal Histogram Regression (CHR) [38] constructs approximately shortest intervals by conformalizing conditional histograms, while Conformal Interquantile Regression (CIR) [19] replaces explicit histograms with interquantile partitions for improved speed. However, these approaches still require approximating a discretized conditional distribution, so the compute-accuracy trade-off is governed by the chosen resolution (number of bins or quantiles) and the fidelity of the underlying multi-quantile estimator. Density/generative-model approaches such as C-HDR [24, 12] can capture multimodality, but they inherit the calibration and stability of the learned predictive density and typically rely on sampling estimates of density ranks; consequently, the resulting prediction set need not be a single interval and may be sensitive to model and Monte Carlo variability.

Complementarily, recent work [15] formalizes *restricted* optimality by constraining admissible sets (e.g., unions of  $k$  intervals), making near-optimal volume achievable via dynamic programming, but again depends on an estimated conditional CDF and discretization choices. Similarly, Conformal Thresholded Intervals (CTI) [30] constructs prediction sets by selecting the shortest interquantile pieces; as highlighted by a comprehensive review [3], although methods like CHR and CIR achieve high efficiency, they inherently trade off simplicity and contiguity, either relying on complex density estimations or yielding non-contiguous sets. Prior to modern CP, direct interval construction via neural networks was explored by [32], who proposed a quality-driven loss using a differentiable sigmoid surrogate to balance coverage and width. However, it relies on a heuristic Lagrangian penalty to govern this trade-off. In contrast, we leverage a similar soft-coverage concept but embeds it within a principled folded geometry. Crucially, CoCP bypasses the complex estimation of the entire conditional CDF or full density. Instead, it only needs to learn a single conditional quantile for the radius; meanwhile, its soft-coverage gradients focus exclusively on the local density near the interval boundaries, autonomously driving the center toward higher-density regions to naturally minimize the required radius.

A separate line of work aims to strengthen coverage beyond marginal guarantees. The necessity of this is underscored by recent diagnostic frameworks [4], which reframe conditional coverage evaluation

as a supervised classification task to formally quantify coverage gaps via the Excess Risk of Target coverage (ERT). Since distribution-free methods cannot, in general, achieve exact conditional coverage uniformly over  $x$  without degenerating to trivial sets [28, 14], many approaches seek principled relaxations via localization, weighting, or restricted shift classes [41, 18, 22]. Conditional calibration methods provide finite-sample conditional guarantees against a user-specified function class, e.g., linear or reproducing kernel Hilbert space (RKHS) reweightings [17]; these guarantees are powerful but are inherently *relative to* the chosen function class and regularization, making practical performance sensitive to kernel and feature design and hyperparameter selection. SpeedCP [25] makes this RKHS-based program computationally practical by tracing the full solution path efficiently, and Conformal Prediction with Length-Optimization (CPL) [27] further incorporates explicit length optimization under the same conditional-constraint viewpoint. For fairness-oriented group guarantees, Kandinsky conformal prediction [2] generalizes class- and covariate-conditional formulations to overlapping and fractional group memberships. Another branch aims to directly minimize the exact conditional coverage error (e.g., Mean Squared Conditional Error [26]); for instance, Colorful Pinball Conformal Prediction (CPCP) [8] utilizes a density-weighted pinball loss to refine the underlying quantile regression. CoCP offers a distinct geometric alternative that we improve conditional reliability by explicitly co-optimizing the interval’s translation and scaling, allowing it to autonomously adapt to local density imbalances.

In addition, several recent methods improve local adaptivity by learning or transforming conformity scores. Rectified Conformal Prediction (RCP) [33] rectifies a base score using an estimate of the conditional score quantile, improving approximate conditional validity while preserving finite-sample marginal validity; related ideas adapt the score using calibration data through split-Jackknife+ constructions [11] or by explicitly training locally adaptive conformal predictors [10]. When instantiated with residual-type scores, these approaches primarily adjust the *scale* of uncertainty and typically do not correct *mis-centering* induced by skewness, since the interval location is inherited from a fixed underlying predictor. Orthogonally, cross-conformal prediction and recent refinements improve statistical efficiency by reusing data and combining fold-wise p-values more effectively [42, 16]. Our approach differs in that we do *not* treat the interval center as fixed: CoCP co-optimizes a center  $m(x)$  and radius  $h(x)$  in an alternating loop, where  $h$  tracks a folded boundary quantile via pinball loss while  $m$  is updated using boundary-local soft-coverage gradients, directly operationalizing the push–pull boundary-balancing mechanism underlying HDI optimality.

### 3 The Geometry of Efficient Intervals

This section establishes the geometric foundation of CoCP. We formalize why the HDI serves as the theoretical lower bound for interval length, and demonstrate how *translating* the interval (i.e., shifting its center) actively reduces the minimal radius required to maintain a  $(1 - \alpha)$  conditional mass. To analyze these dynamics, our central conceptual device is a *folded* representation, which elegantly reduces a two-sided interval boundary into a *single* quantile boundary of a folded residual distribution.

#### 3.1 Setup and the oracle target

Let  $(X, Y) \sim P$  with  $X \in \mathcal{X} \subseteq \mathbb{R}^d$  and  $Y \in \mathbb{R}$ . Write  $F_x$  for the conditional CDF of  $Y | X = x$ , and  $f_x$  for its density when it exists. Fix a miscoverage level  $\alpha \in (0, 1)$ . When  $f_x$  is unimodal and regular, the *shortest* interval achieving a conditional mass of  $1 - \alpha$  is given by:

$$C^*(x) \in \arg \min_{[\ell, u]} \{u - \ell : \mathbb{P}(\ell \leq Y \leq u | X = x) \geq 1 - \alpha\}, \quad (1)$$

which precisely corresponds to the  $(1 - \alpha)$ -HDI. If the optimum is an *interior solution* (i.e., both endpoints lie within the interior of the conditional support), it naturally satisfies the classical equal-density condition  $f_x(\ell^*(x)) = f_x(u^*(x))$ ; see Appendix A.1.

To facilitate a unified geometric analysis, we can also express any interval in a center–radius form. Thus, the oracle  $(1 - \alpha)$  HDI can be written as:

$$C^*(x) = [m^*(x) - h^*(x), m^*(x) + h^*(x)], \quad (2)$$

where  $m^*(x) = (\ell^*(x) + u^*(x))/2$  and  $h^*(x) = (u^*(x) - \ell^*(x))/2$ .

### 3.2 Residual folding

By folding the conditional distribution around a candidate center  $c \in \mathbb{R}$ , we map the two-sided interval problem into a one-sided thresholding problem. The folded residual is defined as  $|Y - c| \mid X = x$ . To achieve a conditional mass of  $1 - \alpha$ , the minimal feasible radius at center  $c$  is:

$$\psi_x(c) := \inf \left\{ r \geq 0 : \mathbb{P}(|Y - c| \leq r \mid X = x) \geq 1 - \alpha \right\}. \quad (3)$$

When the folded residual is continuous, this minimal radius is exactly the  $(1 - \alpha)$ -quantile of the folded distribution:  $Q_{1-\alpha}(|Y - c| \mid X = x)$ .

### 3.3 Why translating the center can shorten the interval

From the folded perspective, finding the HDI is equivalent to searching for the optimal center that minimizes this minimal feasible radius:

$$h^*(x) = \min_{c \in \mathbb{R}} \psi_x(c), \quad m^*(x) \in \arg \min_{c \in \mathbb{R}} \psi_x(c). \quad (4)$$

Under mild smoothness conditions,  $\psi_x(c)$  is differentiable and satisfies the implicit mass constraint:

$$F_x(c + \psi_x(c)) - F_x(c - \psi_x(c)) = 1 - \alpha. \quad (5)$$

Assuming the densities  $f_x(c \pm \psi_x(c))$  exist and their sum is strictly positive, differentiating this implicit equation with respect to  $c$  yields the analytical *push-pull* rule:

$$\psi'_x(c) = - \frac{f_x(c + \psi_x(c)) - f_x(c - \psi_x(c))}{f_x(c + \psi_x(c)) + f_x(c - \psi_x(c))}. \quad (6)$$

This derivative explicitly dictates the interval’s optimal translation dynamic. If the right endpoint  $c + \psi_x(c)$  lies in a region of higher density than the left endpoint  $c - \psi_x(c)$ , the numerator is positive, making  $\psi'_x(c) < 0$ . Consequently, shifting the center  $c$  to the right *decreases* the required radius. At an interior optimal center  $c = m^*(x)$ , the derivative vanishes ( $\psi'_x(m^*(x)) = 0$ ), which perfectly recovers the endpoint density balance  $f_x(m^* + h^*) = f_x(m^* - h^*)$ .

This aligns with the boundary-balancing intuition illustrated in Figure 1c–d. The main takeaway is that constructing an efficient interval naturally decouples into two cooperative tasks:

1. **Scaling:** For any given center  $m(x)$ , the shortest symmetric interval capturing  $1 - \alpha$  mass uses a radius  $\psi_x(m(x))$ , which is exactly the  $(1 - \alpha)$ -quantile of the folded residual.
2. **Translation:** Moving  $m(x)$  toward the denser endpoint strictly reduces the minimal required radius, progressively shortening the interval until the endpoint densities balance.

The next section translates this geometric blueprint into a practical, differentiable learning procedure that bypasses the need to estimate the full conditional density  $f_x$ .

## 4 Co-optimizing Interval Geometry via Alternating Learning

As illustrated in Figure 3, we now introduce CoCP as a coupled learning procedure for a center  $m(x)$  and a radius  $h(x)$ , followed by a split-conformal calibration step. To keep the theoretical exposition transparent, we first present a *split version* in which  $m$  and  $h$  are trained on independent data subsets. Cross-fitting and ensembling are subsequently introduced as practical refinements that reuse data and reduce variance, without compromising the conformal validity argument.

### 4.1 A split version of CoCP

The desired output is an interval parameterized as:

$$C_{m,h}(x) = [m(x) - h(x), m(x) + h(x)]. \quad (7)$$

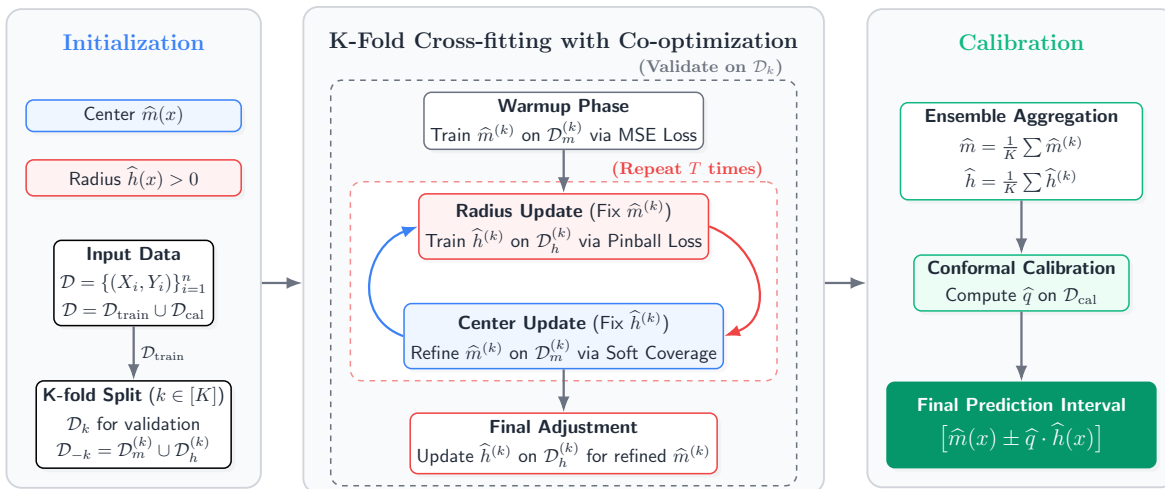


Figure 3: Overview of the CoCP framework. The pipeline begins by parameterizing the prediction interval into a center  $m(x)$  and a radius  $h(x)$ , which are then iteratively refined through an alternating co-optimization process during K-fold cross-fitting. The final adaptive interval is constructed by aggregating the learned components and applying a split-conformal calibration to ensure marginal validity.

In practice,  $m$  and  $h$  can be instantiated as neural networks, with the constraint  $h(x) > 0$  enforced to prevent numerical instability during normalization. Let the available data be partitioned into a training set  $\mathcal{D}_{\text{train}}$  and a calibration set  $\mathcal{D}_{\text{cal}}$ . To facilitate our alternating optimization, we further divide  $\mathcal{D}_{\text{train}}$  into two disjoint subsets,  $\mathcal{D}_m$  and  $\mathcal{D}_h$ , which are used to train the center network  $m$  and the radius network  $h$ , respectively.

Starting from a center initialized via Mean Squared Error (MSE) pre-training, CoCP alternates between two steps: (i) fitting  $h$  as a conditional  $(1 - \alpha)$ -quantile of folded residuals given the current  $m$ ; (ii) refining  $m$  using a boundary-local smooth surrogate of the hard coverage event  $\mathbb{1}\{|Y - m(X)| \leq h(X)\}$ . The process concludes with a final fine-tuning of  $h$  to ensure the radius is optimally scaled to the converged center. This directly implements the scaling and translation discussed in Section 3.

## 4.2 Radius update: folded quantile regression

Fix a current center  $m$ . Motivated by the identity  $\psi_x(m(x)) = Q_{1-\alpha}(|Y - m(X)| \mid X = x)$ , we update  $h$  by performing quantile regression on the folded residual. Define the pinball loss  $\rho_\tau(u) := u(\tau - \mathbb{1}\{u < 0\})$  for  $\tau \in (0, 1)$ . The radius objective is formulated as:

$$\mathcal{L}_H(h; m) := \mathbb{E} \left[ \rho_{1-\alpha}(|Y - m(X)| - h(X)) \right]. \quad (8)$$

Minimizing (8) over all measurable  $h$  yields  $h(x) = Q_{1-\alpha}(|Y - m(X)| \mid X = x)$  under standard conditions.

## 4.3 Center update: boundary-local soft coverage

When  $m$  is suboptimally centered, the endpoints  $m(x) \pm h(x)$  typically sit at different density levels. As established in Section 3, shifting  $m$  toward the denser endpoint reduces the minimal feasible radius. CoCP encourages this shift using a smooth surrogate whose gradients concentrate near the boundary  $|Y - m(X)| \approx h(X)$ .

Let  $\sigma(z) := (1 + \exp(-z))^{-1}$  be the sigmoid function and  $\beta > 0$  be a temperature parameter. Given a fixed radius  $h$ , we define the soft-coverage objective:

$$\mathcal{L}_M(m; h, \beta) := -\mathbb{E} \left[ \sigma \left( \frac{h(X) - |Y - m(X)|}{\beta} \right) \right]. \quad (9)$$

Minimizing  $\mathcal{L}_M$  maximizes a smoothed version of the coverage event. As  $\beta \rightarrow 0^+$ , the derivative of  $\sigma((h - |R|)/\beta)$  concentrates around  $|R| = h$ , producing boundary-local updates.

#### 4.4 Conformal calibration

Given the trained  $\widehat{m}$  and  $\widehat{h}$ , we calibrate them on  $\mathcal{D}_{\text{cal}} = \{(X_i, Y_i)\}_{i=1}^{n_{\text{cal}}}$  using the normalized score:

$$S_i := \frac{|Y_i - \widehat{m}(X_i)|}{\widehat{h}(X_i)}. \quad (10)$$

Let  $\widehat{q}$  be the  $\lceil (n_{\text{cal}} + 1)(1 - \alpha) \rceil$ -th smallest score in  $\{S_i\}_{i=1}^{n_{\text{cal}}}$ . We then output the calibrated interval:

$$\widehat{C}(x) = \left[ \widehat{m}(x) - \widehat{q} \widehat{h}(x), \widehat{m}(x) + \widehat{q} \widehat{h}(x) \right]. \quad (11)$$

This step guarantees exact *marginal* validity in finite samples, regardless of how  $m$  and  $h$  were trained.

#### 4.5 Cross-fitting and ensembling

To use data more efficiently and reduce the variance of the learned geometry, we employ  $K$ -fold cross-fitting. Each fold produces a fitted pair  $(\widehat{m}^{(k)}, \widehat{h}^{(k)})$  trained on the respective training folds. We then aggregate these predictors (e.g., by averaging the network outputs) to obtain the final  $\widehat{m}$  and  $\widehat{h}$ :

$$\widehat{m}(x) := \frac{1}{K} \sum_{k=1}^K \widehat{m}^{(k)}(x), \quad \widehat{h}(x) := \frac{1}{K} \sum_{k=1}^K \widehat{h}^{(k)}(x), \quad (12)$$

and calibrate them on the calibration set. Our complete approach is summarized in Algorithm 1.

*Remark 1.* Cross-fitting and ensembling do not alter the conformal validity argument: the only requirement is that the final functions used to compute the scores are measurable with respect to the training data and independent of the calibration sample. Therefore, for theoretical statements, we focus on the split version described above; the same conclusions apply to cross-fitted and ensembled predictors provided that calibration remains independent.

---

#### Algorithm 1 CoCP: Co-optimization for Adaptive Conformal Prediction

---

**Require:** Training data  $\mathcal{D}_{\text{train}}$ , calibration data  $\mathcal{D}_{\text{cal}}$ , miscoverage  $\alpha$ , folds  $K$ , alternations  $T$ , temperature parameter  $\beta > 0$

**Ensure:** Calibrated interval function  $\widehat{C}(\cdot)$

- 1: **Partition**  $\mathcal{D}_{\text{train}}$  into  $K$  disjoint folds  $\{\mathcal{D}_1, \dots, \mathcal{D}_K\}$
  - 2: Initialize ensemble  $\{(\widehat{m}^{(k)}, \widehat{h}^{(k)})\}_{k=1}^K$
  - 3: **for**  $k = 1, \dots, K$  **do**
  - 4:   Set validation set  $\mathcal{D}_{\text{val}}^{(k)} = \mathcal{D}_k$
  - 5:   **Split**  $\mathcal{D}_{\text{train}} \setminus \mathcal{D}_k$  into two disjoint sets  $\mathcal{D}_m^{(k)}$  and  $\mathcal{D}_h^{(k)}$
  - 6:   Warm-start  $\widehat{m}^{(k)}$  by minimizing MSE on  $\mathcal{D}_m^{(k)}$  while using  $\mathcal{D}_{\text{val}}^{(k)}$  for validation
  - 7:   **for**  $t = 1, \dots, T$  **do**
  - 8:     **Radius update:** fix  $\widehat{m}^{(k)}$ , train  $\widehat{h}^{(k)}$  on  $\mathcal{D}_h^{(k)}$  via pinball loss (8)
  - 9:     **Center update:** fix  $\widehat{h}^{(k)}$ , train  $\widehat{m}^{(k)}$  on  $\mathcal{D}_m^{(k)}$  via soft coverage loss (9) using  $\beta$
  - 10:   **end for**
  - 11:   Fine-tune  $\widehat{h}^{(k)}$  with  $\widehat{m}^{(k)}$  fixed
  - 12: **end for**
  - 13: Form ensemble predictors  $\widehat{m}, \widehat{h}$  via (12)
  - 14: Compute calibration scores  $S_i = |Y_i - \widehat{m}(X_i)|/\widehat{h}(X_i)$  for  $(X_i, Y_i) \in \mathcal{D}_{\text{cal}}$
  - 15: Set  $\widehat{q}$  as the  $\lceil (n_{\text{cal}} + 1)(1 - \alpha) \rceil$ -th smallest score in  $\{S_i\}_{i=1}^{n_{\text{cal}}}$
  - 16: Output  $\widehat{C}(x) = [\widehat{m}(x) - \widehat{q} \cdot \widehat{h}(x), \widehat{m}(x) + \widehat{q} \cdot \widehat{h}(x)]$
-

## 5 Theoretical Properties

This section establishes the theoretical foundations of CoCP. We structure our analysis around three progressive layers of theoretical properties: (i) *finite-sample marginal validity*, which inherently follows from conformal calibration; (ii) the characterization of a temperature-dependent *population target*, which is implicitly induced by the soft-coverage center update; and (iii) *asymptotic efficiency and conditional coverage*, which are achieved as the learning errors vanish and the temperature parameter  $\beta$  approaches zero. All corresponding proofs of the main results are deferred to Appendix A.

### 5.1 Finite-sample marginal validity

**Theorem 1** (Finite-sample marginal coverage). *If the calibration set and a new test sample  $(X, Y)$  are exchangeable conditional on the training fit (i.e., the standard split-conformal setting), then*

$$\mathbb{P}(Y \in \widehat{C}(X)) \geq 1 - \alpha. \quad (13)$$

Theorem 1 is a standard distribution-free result and holds regardless of how  $\widehat{m}$  and  $\widehat{h}$  are trained. The remaining results concern *efficiency* and *conditional reliability*, which do depend on learning and on the temperature  $\beta$ .

### 5.2 Temperature-dependent population target

Recall the conditional soft-coverage functional

$$\Phi_{x,\beta}(c, r) := \mathbb{E} \left[ \sigma \left( \frac{r - |Y - c|}{\beta} \right) \mid X = x \right], \quad \sigma(z) = \frac{1}{1 + e^{-z}}. \quad (14)$$

The derivative of  $\sigma$  induces a symmetric kernel

$$K_\beta(u) := \frac{1}{\beta} \sigma' \left( \frac{u}{\beta} \right), \quad \int_{\mathbb{R}} K_\beta(u) du = 1, \quad (15)$$

and the associated  $\beta$ -smoothed (convolved) density

$$f_{x,\beta}(z) := (f_x * K_\beta)(z) = \int_{\mathbb{R}} f_x(y) K_\beta(z - y) dy. \quad (16)$$

**Lemma 1** (Soft-gradient endpoint imbalance). *Assume  $f_x$  is bounded by  $f_{\max}$ . For any  $c \in \mathbb{R}$ ,  $r > 0$ , and  $\beta > 0$ ,*

$$\frac{\partial}{\partial c} \Phi_{x,\beta}(c, r) = f_{x,\beta}(c + r) - f_{x,\beta}(c - r) + \varepsilon_{x,\beta}(c, r), \quad (17)$$

where

$$|\varepsilon_{x,\beta}(c, r)| \leq 2f_{\max}(1 - \sigma(r/\beta)). \quad (18)$$

Lemma 1 shows that the center update is driven by an endpoint imbalance, but computed on the  $\beta$ -smoothed density  $f_{x,\beta}$  (up to an exponentially small remainder when  $r \gg \beta$ ). This motivates a  $\beta$ -dependent population target. Next recall the folded best-response radius (minimal symmetric radius at center  $c$ )  $\psi_x(c)$  in (3). Under continuity, this is the  $(1 - \alpha)$ -quantile of  $|Y - c| \mid X = x$ .

**Definition 1** ( $\beta$ -soft oracle). Fix  $x$  and  $\beta > 0$ . A pair  $(m_\beta(x), h_\beta(x))$  is a  $\beta$ -soft oracle pair if

$$h_\beta(x) = \psi_x(m_\beta(x)), \quad \frac{\partial}{\partial c} \Phi_{x,\beta}(m_\beta(x), h_\beta(x)) = 0. \quad (19)$$

By Lemma 1, stationarity approximately enforces  $f_{x,\beta}(m_\beta + h_\beta) \approx f_{x,\beta}(m_\beta - h_\beta)$ , i.e., the classical HDI boundary-balance condition but applied to the  $\beta$ -smoothed density  $f_{x,\beta}$ . We would expect this  $\beta$ -soft target to approach the oracle HDI, which will be described by Lemma 2 in the next section.

### 5.3 Asymptotic efficiency and conditional coverage

Let  $n$  and  $n_{\text{cal}}$  denote the sizes of the training and calibration datasets, respectively. Building upon the population-level properties established above, we now present the asymptotic properties for the CoCP framework. These results characterize the behavior of the prediction intervals as the sample size grows, the learning errors vanish, and the temperature parameter  $\beta \rightarrow 0^+$ .

**Assumption 1** (i.i.d. data). The samples are i.i.d. from some unknown joint distribution.

**Assumption 2** (density regularity). For every  $x$ , the conditional distribution  $Y \mid X = x$  admits a Lebesgue density  $f_x$ . For every  $x$ ,  $f_x(y)$  is continuous. Moreover,  $\sup_{x,y} f_x(y) \leq f_{\max} < \infty$ .

**Assumption 3** (unimodality and unique interior HDI). For every  $x$ ,  $f_x$  is unimodal and the unique  $(1 - \alpha)$ -HDI has endpoints  $\ell^*(x), u^*(x)$  that lie in the interior of the support of  $f_x$ .

**Assumption 4** (non-degenerate learned functions). There exist constants  $0 < h_{\min} \leq h_{\max} < \infty$  and  $M < \infty$  such that, with probability tending to one (over  $\mathcal{D}_{\text{train}}$ ), for a fresh  $X$  independent of  $\mathcal{D}_{\text{train}}$ ,  $\widehat{h}(X) \in [h_{\min}, h_{\max}]$ , and  $|\widehat{m}(X)| \leq M$ .

**Assumption 5** (local regularity of the score). Let  $S := |Y - \widehat{m}(X)|/\widehat{h}(X)$  for a fresh  $(X, Y)$  independent of  $\mathcal{D}_{\text{cal}}$ , conditional on  $\mathcal{D}_{\text{train}}$ . There exist constants  $\delta_0 > 0$  and  $s_0 > 0$  such that, with probability tending to one, the conditional density  $f_{S|\mathcal{D}_{\text{train}}}$  exists and satisfies  $f_{S|\mathcal{D}_{\text{train}}}(t) \geq s_0$  for all  $t \in (1 - \delta_0, 1 + \delta_0)$ .

**Assumption 6** (consistency). For any  $\beta > 0$ , there exist sequences  $\eta_{m,n} \rightarrow 0$ ,  $\rho_{m,n} \rightarrow 0$  and  $\eta_{h,n} \rightarrow 0$ ,  $\rho_{h,n} \rightarrow 0$  such that, for a fresh  $X$ ,

$$\mathbb{P}(\mathbb{E}[(\widehat{m}(X) - m_\beta(X))^2 \mid \mathcal{D}_{\text{train}}] \leq \eta_{m,n}) \geq 1 - \rho_{m,n}, \quad (20)$$

$$\mathbb{P}(\mathbb{E}[(\widehat{h}(X) - \psi_X(\widehat{m}(X)))^2 \mid \mathcal{D}_{\text{train}}] \leq \eta_{h,n}) \geq 1 - \rho_{h,n}. \quad (21)$$

**Lemma 2** (Vanishing  $\beta$ -bias of the  $\beta$ -soft oracle). Fix  $x \in \mathcal{X}$  and let  $m^*(x)$  denote the oracle  $(1 - \alpha)$ -HDI center, with oracle radius  $h^*(x) := \psi_x(m^*(x))$ . Under Assumptions 2 and 3, any  $\beta$ -soft oracle pair  $(m_\beta(x), h_\beta(x))$  in Definition 1 satisfies

$$m_\beta(x) \rightarrow m^*(x), \quad h_\beta(x) \rightarrow h^*(x), \quad \text{as } \beta \rightarrow 0^+. \quad (22)$$

**Theorem 2** (Asymptotic optimal length and conditional coverage). Under Assumptions 1–6, and along any deterministic sequence  $\beta = \beta_n \rightarrow 0^+$ , the split-calibrated CoCP interval  $\widehat{C}(x)$  satisfies:  
(i) Calibration factor vanishes asymptotically:

$$|\widehat{q} - 1| = O_{\mathbb{P}}\left(\sqrt{\eta_{h,n}} + \sqrt{\frac{\log n_{\text{cal}}}{n_{\text{cal}}}}\right), \quad \text{hence } \widehat{q} \xrightarrow{\mathbb{P}} 1. \quad (23)$$

(ii) Asymptotic conditional coverage: there exist random sets  $\Lambda_n \subseteq \mathcal{X}$  with  $\mathbb{P}(X \in \Lambda_n) \rightarrow 1$  such that

$$\sup_{x \in \Lambda_n} \left| \mathbb{P}(Y \in \widehat{C}(x) \mid X = x) - (1 - \alpha) \right| \xrightarrow{\mathbb{P}} 0. \quad (24)$$

(iii) Oracle-efficient length: for a fresh  $X$ ,

$$|\widehat{C}(X)| - |C^*(X)| \xrightarrow{\mathbb{P}} 0. \quad (25)$$

Moreover, the gap to the oracle HDI admits the explicit pointwise decomposition

$$|\widehat{C}(x)| - |C^*(x)| \leq 2|\widehat{q} - 1|\widehat{h}(x) + 2|\widehat{h}(x) - \psi_x(\widehat{m}(x))| + 2|\widehat{m}(x) - m_{\beta_n}(x)| + 2|m_{\beta_n}(x) - m^*(x)|. \quad (26)$$

The decomposition in (26) elegantly decouples the sources of inefficiency:

- The **radius estimation error**  $|\widehat{h}(x) - \psi_x(\widehat{m}(x))|$ , together with the calibration error  $|\widehat{q} - 1|$ , primarily dictates *conditional coverage* reliability.

- The **center estimation error**  $|\widehat{m}(x) - m_{\beta_n}(x)|$  dictates how well learning matches the population target induced by the  $\beta_n$ -soft objective.
- The final term  $|m_{\beta_n}(x) - m^*(x)|$  is a **vanishing  $\beta_n$ -bias**: it quantifies the discrepancy between the  $\beta_n$ -soft boundary-balancing target and the true HDI center. When  $\beta_n \rightarrow 0^+$ , this bias disappears.

*Remark 2.* Lemma 2 establishes that the  $\beta$ -soft oracle target converges to the oracle  $(1 - \alpha)$ -HDI as  $\beta \rightarrow 0^+$ , which is the only population-level ingredient needed to make the last term in the length decomposition (26) vanish along any  $\beta_n \rightarrow 0^+$ . In addition, one can sharpen the *rate* of this  $\beta$ -bias under extra local smoothness assumptions. Specifically, if  $f_x$  is locally twice continuously differentiable in neighborhoods of the oracle HDI endpoints and the endpoints are non-flat (e.g.,  $f'_x(\ell^*(x)) > 0$  and  $f'_x(u^*(x)) < 0$ ), then kernel symmetry implies a *second-order* interior bias:

$$|m_\beta(x) - m^*(x)| = O(\beta^2), \quad |h_\beta(x) - h^*(x)| = O(\beta^2). \quad (27)$$

By contrast, when the oracle HDI is pinned at an active support boundary, the  $\beta$ -soft oracle remains consistent but exhibits an explicit *first-order*  $O(\beta)$  boundary shift. In both regimes, the bias still vanishes as long as  $\beta_n \rightarrow 0^+$ , hence the asymptotic optimality and conditional coverage conclusions of Theorem 2 remain unchanged. We defer the precise statements and proofs to Appendix B.

## 6 Experiments

**Protocol and implementation.** We evaluate CoCP on (i) controlled synthetic benchmarks with known conditional distributions and (ii) real-world regression datasets. Unless otherwise stated, we target nominal coverage  $1 - \alpha = 0.9$  (i.e.,  $\alpha = 0.1$ ) and report mean (standard deviation) over 10 independent random splits. Each split follows a partition of the available data into train/calibration/test with ratios 60%/20%/20%. And 16.7% of the training set is used for validation and early stopping, while the calibration set is used for conformal calibration. To ensure a fair comparison, *all* learning-based components across methods use the same backbone architecture: a two-hidden-layer MLP with 64 ReLU units per layer. All models are trained with early stopping (patience 100, max 1000 epochs) and mini-batches of size 512. More implementation details are provided in Appendix C.

**Baselines.** We compare against standard residual-based split conformal prediction (Split [31]), CQR [35], distributional-set baselines (C-HDR [24, 12], CHR [38]), and conditional-coverage-oriented methods (CPL [27], CPCP [8], RCP [33]). Due to the prohibitive computational cost of RKHS-based conditional conformal method [17], we include a simplified version without test imputation, denoted as Naive CC, exclusively on synthetic data.

**Metrics.** We always report marginal coverage and mean interval width (Length). To quantify conditional reliability, on synthetic data we exploit the known conditional CDF to compute the exact conditional coverage at each test covariate and report the mean absolute deviation from the target  $1 - \alpha$  (ConMAE). On real data, where the conditional distribution is unknown, we report diagnostic surrogates: Mean Squared Conditional Error (MSCE [26]), Worst-Slice Coverage (WSC [7, 36]), and excess risk of the target coverage (ERT [4]), including  $\ell_1$ -ERT and  $\ell_2$ -ERT. Formal definitions and estimator details are provided in Appendix C.5.

### 6.1 Synthetic data

**Setup.** We define a shared covariate distribution  $X \sim \text{Unif}([-2, 2])$  and two structural functions: a location function  $\theta(x) = \frac{1}{2} \sin(1.5x)$  and a heteroscedastic scale function  $s(x) = 0.15 + 0.25x^2$ . The response variable is generated as  $Y = \theta(X) + \eta(X, \epsilon)$ , where the noise term  $\eta$  instantiates three distinct families to cover symmetric, moderately skewed, and highly skewed conditional distributions:

- **Normal:**  $\eta = s(X) \cdot \epsilon$  with  $\epsilon \sim \mathcal{N}(0, 1)$ .
- **Exponential:**  $\eta \sim \text{Exp}(\lambda = 1/s(X))$ , shifting the support to  $[\theta(X), \infty)$ .
- **Log-Normal:**  $\eta = s(X)(\epsilon - e^{-\sigma^2})$  with  $\epsilon \sim \text{LogNormal}(0, \sigma^2)$ , where the mode is at  $\theta(X)$ .

We set  $n = 20,000$  and  $\sigma = 0.6$  for all experiments. For reference, we include the **Oracle** interval, defined as the true  $(1 - \alpha)$ -HDI under the known conditional distribution.

**Main results.** Table 1 summarizes the results. Across all three synthetic benchmarks, CoCP attains the *smallest* conditional-coverage error (ConMAE), indicating the most reliable conditional behavior among practical methods while maintaining nominal marginal coverage.

The gains of co-optimizing *translation* and *scaling* are most pronounced under skewness. On Log-Normal noise, CoCP substantially reduces average length relative to equal-tailed baselines (e.g., a  $\approx 13\%$  reduction vs. CQR) while also nearly halving ConMAE. On the highly skewed Exponential benchmark, CoCP yields the tightest non-oracle intervals, reducing length over CQR by  $\approx 20\%$  and reducing ConMAE by  $\approx 60\%$ . These improvements align with our geometric motivation: when endpoint densities are imbalanced, *re-centering* the interval is essential for approaching HDI-like efficiency.

**Qualitative geometry.** Figures 4-6 visualize learned intervals against the oracle HDI. Under symmetric Gaussian noise (Figure 4), most adaptive methods achieve comparable geometry, and CoCP remains competitive. Under skewed LogNormal and Exponential noise (Figures 5 and 6), center-invariant constructions exhibit systematic mis-centering, whereas CoCP explicitly shifts the center toward higher-density regions and contracts the radius accordingly, yielding a closer match to the oracle bounds.

Table 1: Experimental results on synthetic datasets (mean  $\pm$  std over 10 splits,  $\alpha = 0.1$ ). Lower **Length** and **ConMAE** are better. The Oracle row reports the true  $(1 - \alpha)$ -HDI for reference.

Dataset	Method	Coverage	Length ( $\downarrow$ )	ConMAE ( $\downarrow$ )
Normal	Oracle	0.9000 (0.0000)	1.5922 (0.0101)	0.0000 (0.0000)
	Split	0.8995 (0.0050)	1.8735 (0.0404)	0.1119 (0.0030)
	CPL	0.9004 (0.0103)	<b>1.5055 (0.0456)</b>	0.0768 (0.0071)
	Naive CC	0.9001 (0.0033)	1.5902 (0.0159)	0.0093 (0.0021)
	CQR	0.9016 (0.0041)	1.5989 (0.0165)	0.0095 (0.0026)
	CPCP	0.9026 (0.0120)	1.6050 (0.0335)	0.0180 (0.0051)
	RCP	0.9007 (0.0048)	1.5973 (0.0367)	0.0142 (0.0029)
	C-HDR	0.9014 (0.0038)	1.6012 (0.0280)	0.0084 (0.0014)
	CHR	0.9029 (0.0024)	1.6228 (0.0150)	0.0107 (0.0048)
	CoCP	0.9002 (0.0039)	1.5962 (0.0180)	<b>0.0066 (0.0015)</b>
LogNormal	Oracle	0.9000 (0.0000)	0.9591 (0.0061)	0.0000 (0.0000)
	Split	0.9000 (0.0051)	1.2377 (0.0301)	0.0964 (0.0036)
	CPL	0.9009 (0.0046)	0.9739 (0.0227)	0.0510 (0.0037)
	Naive CC	0.9001 (0.0028)	0.9694 (0.0171)	0.0078 (0.0025)
	CQR	0.9010 (0.0035)	1.1110 (0.0352)	0.0122 (0.0050)
	CPCP	0.9018 (0.0166)	0.9955 (0.0461)	0.0190 (0.0080)
	RCP	0.9010 (0.0048)	0.9723 (0.0273)	0.0123 (0.0042)
	C-HDR	0.8999 (0.0021)	0.9752 (0.0201)	0.0103 (0.0036)
	CHR	0.9039 (0.0059)	0.9983 (0.0213)	0.0114 (0.0023)
	CoCP	0.9007 (0.0032)	<b>0.9621 (0.0138)</b>	<b>0.0064 (0.0012)</b>
Exponential	Oracle	0.9000 (0.0000)	1.1145 (0.0070)	0.0000 (0.0000)
	Split	0.8989 (0.0031)	1.5679 (0.0217)	0.0937 (0.0036)
	CPL	0.8969 (0.0076)	1.1530 (0.0409)	0.0345 (0.0061)
	Naive CC	0.8962 (0.0029)	1.2270 (0.0431)	0.0092 (0.0026)
	CQR	0.8975 (0.0031)	1.4222 (0.0171)	0.0172 (0.0042)
	CPCP	0.8926 (0.0108)	1.2215 (0.0622)	0.0160 (0.0068)
	RCP	0.9000 (0.0048)	1.2468 (0.0362)	0.0111 (0.0035)
	C-HDR	0.8964 (0.0028)	1.2359 (0.0420)	0.0074 (0.0022)
	CHR	0.9019 (0.0025)	1.1662 (0.0157)	0.0113 (0.0023)
	CoCP	0.8973 (0.0029)	<b>1.1351 (0.0142)</b>	<b>0.0069 (0.0015)</b>

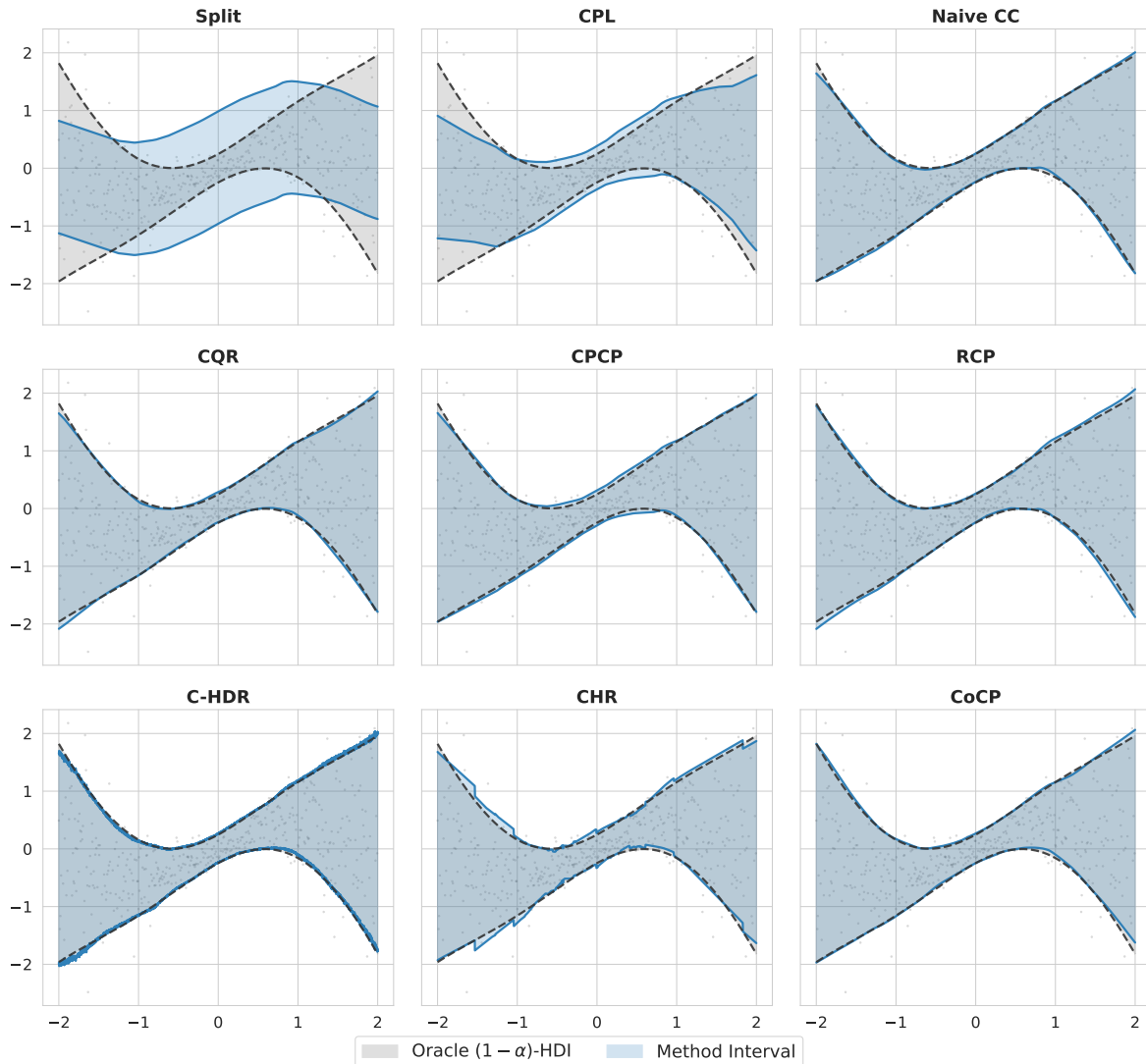


Figure 4: **Prediction intervals on the synthetic Normal dataset.** This visualization compares nine conformal methods under symmetric, heteroscedastic Gaussian noise. The gray area denotes the Oracle  $(1 - \alpha)$ -HDI. Most adaptive methods, including CoCP, successfully capture the symmetric uncertainty, while the Split baseline (top-left) produces overly conservative, non-adaptive intervals.

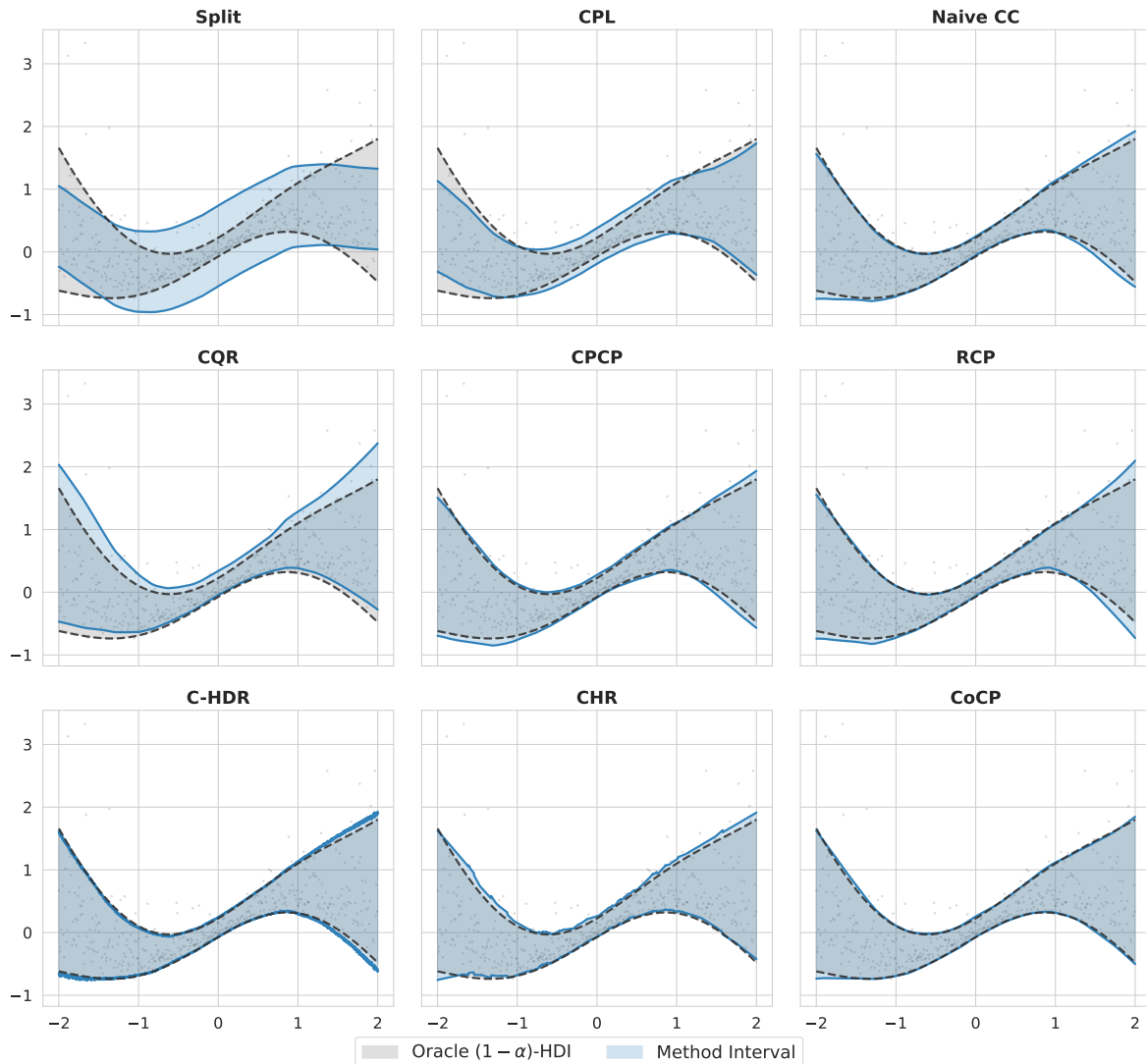


Figure 5: **Prediction intervals on the synthetic LogNormal dataset.** Under skewed conditional noise, the discrepancy between center-invariant methods (e.g., CQR) and the Oracle HDI (gray) becomes prominent. CoCP (bottom-right) demonstrates its ability to shift the interval center and scale the radius simultaneously, resulting in a geometry that closely aligns with the Oracle’s bounds.

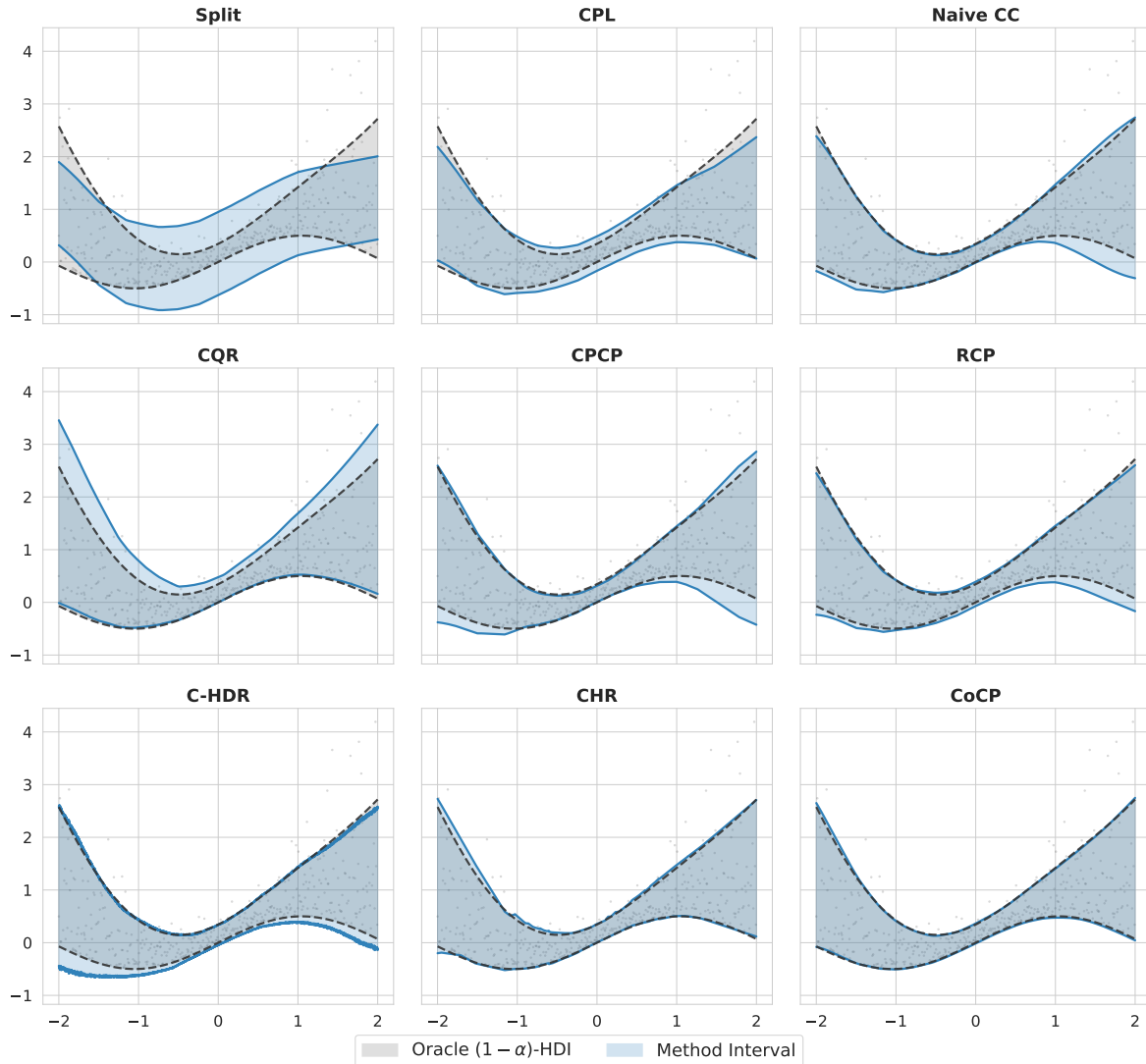


Figure 6: **Prediction intervals on the synthetic Exponential dataset.** This case represents extreme skewness. While methods like RCP remain centered around the conditional mean, CoCP effectively utilizes the boundary-balancing mechanism to push the interval toward the high-density region near the lower bound, achieving significantly shorter lengths while maintaining valid coverage.

## 6.2 Real data

**Setup.** We evaluate on seven commonly used real-world regression datasets spanning different feature dimensions and noise characteristics: *bike*, *bio*, *blog*, *facebook-1*, *facebook-2*, *homes*, and *supercon*. (summarized in Table 2). We follow the same split protocol and neural architecture standardization as above. Because true conditional coverage is unavailable, we report both efficiency measure (length) and conditional-reliability diagnostics (MSCE/WSC/ERT).

Table 2: Overview of the real-world datasets used in our study.  $n$  and  $d$  represent the number of samples and features, respectively.

Dataset	Description	Samples ( $n$ )	Dim ( $d$ )	Ref.
<i>bike</i>	Hourly bike sharing demand	10,886	18	[13]
<i>bio</i>	Protein tertiary structure properties	45,730	9	[34]
<i>blog</i>	Blog feedback volume prediction	52,397	280	[5]
<i>facebook-1</i>	Facebook comment volume (Variant 1)	40,948	53	[40]
<i>facebook-2</i>	Facebook comment volume (Variant 2)	81,311	53	[40]
<i>homes</i>	King County house sales prices	21,613	19	[21]
<i>supercon.</i>	Superconductivity critical temperature	21,263	81	[20]

**Main results.** Table 3 reports the results. CoCP achieves the shortest intervals on 5 out of 7 datasets while maintaining coverage close to the nominal level. On the remaining two datasets (*blog* and *facebook-2*), CHR attains slightly shorter intervals but CoCP demonstrates markedly superior conditional reliability (substantially lower MSCE and ERT, and higher WSC), suggesting that CoCP refines the spatial distribution of coverage, achieving a better efficiency-reliability trade-off than methods that focus solely on minimizing average width.

Beyond length, CoCP consistently improves conditional diagnostics: it attains the lowest  $\ell_1$ -ERT on 6 out of 7 datasets (and is competitive on the remaining one), and the lowest  $\ell_2$ -ERT on all datasets up to small-sample estimation noise. This pattern supports the central claim of CoCP that coupling center translation with radius learning reduces systematic local miscoverage that is otherwise detectable by conditional-coverage auditors, while preserving the marginal conformal guarantee.

## 7 Conclusions

This work presented CoCP, a conformal regression method that explicitly couples translation and scaling. The method is motivated by a folded-residual geometry: for any chosen center, the shortest interval achieving the nominal conditional mass is determined by a single boundary quantile of the absolute residual, and shifting the center toward the higher-density boundary reduces the required radius. CoCP turns this principle into a practical alternating procedure through quantile regression for the radius and boundary-local soft-coverage updates for the center, followed by a standard split-conformal calibration that preserves finite-sample marginal coverage. Crucially, this geometric alignment allows CoCP to theoretically approach the optimal highest-density interval. Empirically, this translates to a superior efficiency-reliability trade-off, as CoCP yields significantly tighter prediction bands and state-of-the-art conditional coverage diagnostics compared to existing baselines.

A natural direction is extending the co-optimization viewpoint beyond one-dimensional responses. In higher-dimensional outputs, one still would like to parameterize a center and a nonconformity-guided scale. However, many efficient multi-output conformal regression pipelines rely on generative or representation-based constructions [12]. For example, mapping data to a latent Gaussian space via conditional flows, or using auto-encoding representations. In such settings, the latent center may not correspond to an interpretable region in the original space, and translating the latent center need not be size-invariant after decoding because local geometric distortion (e.g., Jacobian variation or non-invertibility) can change the induced set volume and shape. This suggests two complementary paths: (1) direct output-space parameterizations (e.g., ellipsoids or other translation-invariant families) where center shifts do not alter size by construction, and (2) invertible generative parameterizations

Table 3: Experimental results on real-world datasets (mean  $\pm$  std over 10 splits,  $\alpha = 0.1$ ). We report coverage and average length, plus conditional-coverage diagnostics (MSCE, WSC at  $\delta = 0.1$ , and  $\ell_1/\ell_2$ -ERT). Best values per dataset/metric (excluding Coverage) are highlighted in bold.

Dataset	Method	Coverage	Length ( $\downarrow$ )	MSCE ( $\downarrow$ )	WSC ( $\uparrow$ )	$\ell_1$ -ERT ( $\downarrow$ )	$\ell_2$ -ERT ( $\downarrow$ )
<i>bike</i>	Split	0.8980 (0.0111)	0.7700 (0.0360)	0.0041 (0.0016)	0.6974 (0.0259)	0.0663 (0.0063)	0.0080 (0.0022)
	CPL	0.9146 (0.0100)	0.7938 (0.0373)	0.0021 (0.0015)	0.7800 (0.0515)	0.0369 (0.0087)	0.0022 (0.0023)
	CQR	0.8993 (0.0040)	0.7856 (0.1255)	0.0018 (0.0006)	0.7573 (0.0180)	0.0350 (0.0127)	0.0020 (0.0015)
	CPCP	0.9030 (0.0162)	0.7475 (0.0515)	0.0010 (0.0003)	<b>0.7933 (0.0251)</b>	0.0206 (0.0090)	0.0003 (0.0007)
	RCP	0.9014 (0.0096)	0.7497 (0.0474)	0.0013 (0.0006)	0.7787 (0.0158)	0.0250 (0.0125)	0.0008 (0.0009)
	C-HDR	0.8994 (0.0091)	0.7610 (0.0325)	0.0015 (0.0005)	0.7752 (0.0114)	0.0258 (0.0136)	0.0013 (0.0014)
	CHR	0.9067 (0.0122)	0.7018 (0.0349)	0.0013 (0.0004)	0.7919 (0.0218)	0.0279 (0.0095)	0.0011 (0.0007)
	CoCP	0.8996 (0.0061)	<b>0.6606 (0.0201)</b>	<b>0.0008 (0.0004)</b>	0.7917 (0.0110)	<b>0.0181 (0.0080)</b>	<b>0.0001 (0.0007)</b>
<i>bio</i>	Split	0.9032 (0.0049)	1.7584 (0.0301)	0.0006 (0.0002)	0.8258 (0.0070)	0.0241 (0.0044)	0.0009 (0.0003)
	CPL	0.9057 (0.0081)	1.6358 (0.0449)	0.0005 (0.0002)	0.8438 (0.0130)	0.0161 (0.0042)	0.0004 (0.0003)
	CQR	0.8986 (0.0052)	1.5251 (0.0164)	0.0003 (0.0001)	0.8455 (0.0079)	0.0088 (0.0028)	0.0001 (0.0001)
	CPCP	0.9048 (0.0072)	1.6452 (0.0413)	0.0004 (0.0002)	<b>0.8463 (0.0119)</b>	0.0134 (0.0049)	0.0002 (0.0002)
	RCP	0.9013 (0.0042)	1.6355 (0.0265)	0.0003 (0.0003)	0.8403 (0.0090)	<b>0.0074 (0.0063)</b>	0.0003 (0.0004)
	C-HDR	0.9019 (0.0044)	1.5598 (0.0292)	0.0006 (0.0004)	0.8330 (0.0148)	0.0177 (0.0069)	0.0006 (0.0004)
	CHR	0.9017 (0.0072)	1.5145 (0.0350)	0.0003 (0.0001)	0.8460 (0.0097)	0.0106 (0.0044)	0.0001 (0.0001)
	CoCP	0.9017 (0.0038)	<b>1.4140 (0.0133)</b>	<b>0.0002 (0.0001)</b>	0.8446 (0.0098)	0.0086 (0.0056)	<b>0.0001 (0.0001)</b>
<i>blog</i>	Split	0.8998 (0.0040)	3.7416 (0.0604)	0.0048 (0.0007)	0.7349 (0.0140)	0.0726 (0.0043)	0.0068 (0.0015)
	CPL	0.9179 (0.0069)	3.7549 (0.1810)	0.0012 (0.0004)	<b>0.8503 (0.0093)</b>	0.0377 (0.0060)	-0.0000 (0.0008)
	CQR	0.8973 (0.0027)	2.7947 (0.1018)	0.0014 (0.0004)	0.8087 (0.0101)	0.0300 (0.0048)	-0.0007 (0.0007)
	CPCP	0.8992 (0.0061)	3.3285 (0.0708)	0.0005 (0.0003)	0.8328 (0.0137)	0.0353 (0.0075)	0.0003 (0.0013)
	RCP	0.8980 (0.0043)	3.3837 (0.0917)	0.0008 (0.0004)	0.8154 (0.0130)	0.0359 (0.0037)	0.0009 (0.0009)
	C-HDR	0.8977 (0.0025)	3.1149 (0.2137)	0.0011 (0.0008)	0.8223 (0.0220)	0.0271 (0.0070)	-0.0005 (0.0012)
	CHR	0.9093 (0.0049)	<b>2.5531 (0.0744)</b>	0.0006 (0.0003)	0.8479 (0.0117)	0.0208 (0.0047)	-0.0018 (0.0006)
	CoCP	0.8989 (0.0044)	2.7080 (0.1242)	<b>0.0004 (0.0001)</b>	0.8393 (0.0071)	<b>0.0177 (0.0029)</b>	<b>-0.0019 (0.0005)</b>
<i>facebook-1</i>	Split	0.9012 (0.0053)	2.1838 (0.0341)	0.0021 (0.0004)	0.7814 (0.0154)	0.0547 (0.0051)	0.0037 (0.0009)
	CPL	0.8993 (0.0069)	1.8935 (0.0756)	0.0004 (0.0002)	0.8425 (0.0090)	0.0172 (0.0061)	0.0002 (0.0005)
	CQR	0.8984 (0.0060)	1.7500 (0.0462)	0.0008 (0.0003)	0.8144 (0.0099)	0.0249 (0.0074)	0.0006 (0.0007)
	CPCP	0.8991 (0.0053)	1.9626 (0.0567)	0.0005 (0.0003)	0.8252 (0.0197)	0.0235 (0.0108)	0.0005 (0.0011)
	RCP	0.8998 (0.0049)	1.9151 (0.0394)	0.0003 (0.0001)	0.8395 (0.0117)	0.0146 (0.0049)	0.0000 (0.0004)
	C-HDR	0.9006 (0.0027)	1.8299 (0.0381)	0.0007 (0.0005)	0.8287 (0.0148)	0.0158 (0.0074)	0.0002 (0.0008)
	CHR	0.9059 (0.0052)	1.6920 (0.0344)	0.0006 (0.0002)	0.8297 (0.0074)	0.0188 (0.0080)	-0.0001 (0.0003)
	CoCP	0.8993 (0.0046)	<b>1.6269 (0.0284)</b>	<b>0.0002 (0.0001)</b>	<b>0.8472 (0.0065)</b>	<b>0.0087 (0.0045)</b>	<b>-0.0004 (0.0003)</b>
<i>facebook-2</i>	Split	0.8991 (0.0026)	2.0821 (0.0192)	0.0015 (0.0004)	0.7964 (0.0080)	0.0560 (0.0026)	0.0035 (0.0006)
	CPL	0.8973 (0.0034)	1.7975 (0.0381)	0.0002 (0.0001)	0.8482 (0.0093)	0.0155 (0.0037)	0.0003 (0.0003)
	CQR	0.8977 (0.0036)	1.6684 (0.0315)	0.0006 (0.0004)	0.8269 (0.0124)	0.0246 (0.0057)	0.0007 (0.0005)
	CPCP	0.8994 (0.0026)	1.8508 (0.0430)	0.0003 (0.0002)	0.8433 (0.0148)	0.0208 (0.0098)	0.0006 (0.0008)
	RCP	0.8996 (0.0031)	1.8083 (0.0380)	0.0003 (0.0001)	0.8477 (0.0089)	0.0160 (0.0028)	0.0004 (0.0002)
	C-HDR	0.8986 (0.0017)	1.7364 (0.0254)	0.0004 (0.0002)	0.8402 (0.0096)	0.0206 (0.0045)	0.0005 (0.0003)
	CHR	0.9020 (0.0032)	<b>1.4582 (0.0400)</b>	0.0005 (0.0002)	0.8361 (0.0089)	0.0230 (0.0033)	0.0004 (0.0002)
	CoCP	0.8987 (0.0021)	1.5156 (0.0188)	<b>0.0001 (0.0001)</b>	<b>0.8554 (0.0042)</b>	<b>0.0113 (0.0024)</b>	<b>-0.0001 (0.0001)</b>
<i>homes</i>	Split	0.9000 (0.0087)	0.5964 (0.0287)	0.0112 (0.0016)	0.5788 (0.0302)	0.0931 (0.0044)	0.0191 (0.0022)
	CPL	0.9087 (0.0119)	0.6331 (0.0377)	0.0009 (0.0004)	0.7909 (0.0335)	0.0357 (0.0093)	0.0021 (0.0015)
	CQR	0.9034 (0.0059)	0.5664 (0.0189)	0.0007 (0.0005)	0.8192 (0.0158)	0.0118 (0.0078)	0.0003 (0.0006)
	CPCP	0.8978 (0.0094)	0.5888 (0.0212)	0.0009 (0.0007)	0.7984 (0.0413)	0.0201 (0.0117)	0.0007 (0.0012)
	RCP	0.8992 (0.0047)	0.5845 (0.0204)	0.0006 (0.0004)	0.8020 (0.0207)	0.0169 (0.0082)	0.0008 (0.0009)
	C-HDR	0.9003 (0.0043)	0.5372 (0.0155)	0.0007 (0.0003)	0.8211 (0.0096)	0.0086 (0.0061)	-0.0001 (0.0004)
	CHR	0.9013 (0.0091)	0.5428 (0.0165)	0.0007 (0.0006)	0.8199 (0.0152)	0.0149 (0.0085)	0.0002 (0.0007)
	CoCP	0.9024 (0.0070)	<b>0.5257 (0.0093)</b>	<b>0.0003 (0.0002)</b>	<b>0.8270 (0.0127)</b>	<b>0.0070 (0.0096)</b>	<b>-0.0003 (0.0004)</b>
<i>supercon.</i>	Split	0.9036 (0.0065)	1.0186 (0.0442)	0.0066 (0.0010)	0.7061 (0.0246)	0.0875 (0.0035)	0.0088 (0.0009)
	CPL	0.9068 (0.0134)	0.9371 (0.0325)	0.0012 (0.0005)	0.8074 (0.0298)	0.0333 (0.0093)	0.0015 (0.0014)
	CQR	0.9013 (0.0072)	0.9059 (0.0345)	0.0006 (0.0002)	0.8094 (0.0104)	0.0211 (0.0069)	0.0000 (0.0007)
	CPCP	0.8971 (0.0124)	0.9186 (0.0426)	0.0007 (0.0007)	0.7998 (0.0371)	0.0269 (0.0084)	0.0007 (0.0015)
	RCP	0.9049 (0.0069)	0.9695 (0.0393)	0.0007 (0.0004)	0.8125 (0.0187)	0.0236 (0.0113)	0.0004 (0.0014)
	C-HDR	0.9048 (0.0063)	1.0638 (0.0457)	<b>0.0003 (0.0002)</b>	0.8202 (0.0129)	0.0211 (0.0071)	-0.0000 (0.0005)
	CHR	0.9131 (0.0063)	0.9875 (0.0396)	0.0013 (0.0004)	0.8111 (0.0140)	0.0287 (0.0053)	0.0003 (0.0007)
	CoCP	0.9033 (0.0054)	<b>0.7848 (0.0136)</b>	0.0004 (0.0001)	<b>0.8244 (0.0046)</b>	<b>0.0142 (0.0050)</b>	<b>-0.0005 (0.0005)</b>

paired with objectives or regularizers that control distortion if efficiency is evaluated in the original space. Developing co-optimization schemes with principled geometry and efficiency guarantees for multivariate and structured outputs remains an important open problem.

## A Main Theoretical Proofs

### A.1 HDI endpoint density equality

**Proposition 1.** *Fix  $x$  and assume  $Y | X = x$  has a continuous density  $f_x$ . Let  $(\ell^*(x), u^*(x))$  be any solution to*

$$(\ell^*(x), u^*(x)) \in \arg \min_{\ell < u} \left\{ u - \ell : \int_{\ell}^u f_x(y) dy \geq 1 - \alpha \right\}.$$

*If the optimum is an interior solution (i.e., it does not occur at the boundary of the support), then the optimal interval has exact mass  $1 - \alpha$ , and its endpoints satisfy the density balance condition:*

$$f_x(\ell^*(x)) = f_x(u^*(x)).$$

*Proof.* Suppose for contradiction that the optimal interval satisfies  $\int_{\ell^*}^{u^*} f_x(y) dy > 1 - \alpha$ . By the continuity of  $f_x$ , we could slightly shrink the interval (e.g., increase  $\ell^*$ ) to strictly decrease its length while maintaining the  $1 - \alpha$  mass constraint, which contradicts optimality. Thus, the constraint must bind.

To find the optimal interior endpoints, we minimize the length  $u - \ell$  subject to this binding constraint. The Lagrangian is:

$$\mathcal{L}(\ell, u, \lambda) = (u - \ell) + \lambda \left( \int_{\ell}^u f_x(y) dy - (1 - \alpha) \right).$$

Setting the partial derivatives to zero yields:

$$\frac{\partial \mathcal{L}}{\partial u} = 1 + \lambda f_x(u^*) = 0, \quad \frac{\partial \mathcal{L}}{\partial \ell} = -1 - \lambda f_x(\ell^*) = 0.$$

Eliminating  $\lambda$  immediately gives  $f_x(\ell^*) = f_x(u^*)$ . □

### A.2 Proof of Lemma 1

*Proof.* Fix  $x$ . Write

$$\Phi_{x,\beta}(c, r) = \int \sigma \left( \frac{r - |y - c|}{\beta} \right) f_x(y) dy.$$

Since  $f_x$  is bounded and  $\sigma'$  is integrable, we may differentiate under the integral sign by dominated convergence. Indeed, for all  $y \neq c$ ,

$$\left| \frac{\partial}{\partial c} \sigma \left( \frac{r - |y - c|}{\beta} \right) \right| \leq \frac{1}{\beta} \sigma' \left( \frac{c + r - y}{\beta} \right) + \frac{1}{\beta} \sigma' \left( \frac{c - r - y}{\beta} \right),$$

and therefore the derivative integrand is dominated by  $f_{\max}(K_{\beta}(c + r - y) + K_{\beta}(c - r - y))$ , whose integral over  $y$  equals  $2f_{\max}$ . Then

$$\frac{\partial}{\partial c} \Phi_{x,\beta}(c, r) = \int \frac{1}{\beta} \sigma' \left( \frac{r - |y - c|}{\beta} \right) \text{sign}(y - c) f_x(y) dy.$$

Split the integral into  $y \geq c$  and  $y < c$ .

For  $y \geq c$ :  $|y - c| = y - c$ ,  $\text{sign}(y - c) = +1$ . Thus

$$\begin{aligned} I_+(c) &:= \int_c^{\infty} \frac{1}{\beta} \sigma' \left( \frac{c + r - y}{\beta} \right) f_x(y) dy \\ &= f_{x,\beta}(c + r) - \int_{-\infty}^c \frac{1}{\beta} \sigma' \left( \frac{c + r - y}{\beta} \right) f_x(y) dy \\ &= f_{x,\beta}(c + r) - \int_{r/\beta}^{\infty} \sigma'(t) f_x(c + r - \beta t) dt \quad \left( \text{with } t = \frac{c + r - y}{\beta} \right). \end{aligned}$$

For  $y < c$ :  $|y - c| = c - y$ ,  $\text{sign}(y - c) = -1$ . Thus

$$\begin{aligned}
I_-(c) &:= - \int_{-\infty}^c \frac{1}{\beta} \sigma' \left( \frac{r - (c - y)}{\beta} \right) f_x(y) dy \\
&= - \int_{-\infty}^c \frac{1}{\beta} \sigma' \left( \frac{c - r - y}{\beta} \right) f_x(y) dy \\
&= -f_{x,\beta}(c - r) + \int_c^{\infty} \frac{1}{\beta} \sigma' \left( \frac{c - r - y}{\beta} \right) f_x(y) dy \\
&= -f_{x,\beta}(c - r) + \int_{r/\beta}^{\infty} \sigma'(t) f_x(c - r + \beta t) dt \quad \left( \text{with } t = \frac{y - (c - r)}{\beta} \right).
\end{aligned}$$

Summing yields

$$\frac{\partial}{\partial c} \Phi_{x,\beta}(c, r) = f_{x,\beta}(c + r) - f_{x,\beta}(c - r) + \int_{r/\beta}^{\infty} \sigma'(t) (f_x(c - r + \beta t) - f_x(c + r - \beta t)) dt.$$

Using  $|f_x| \leq f_{\max}$  and  $\int_{r/\beta}^{\infty} \sigma'(t) dt = 1 - \sigma(r/\beta)$  yields the remainder bound.  $\square$

### A.3 Proof of Theorem 1

*Proof.* Condition on  $\mathcal{D}_{\text{train}}$ ; then  $\hat{m}, \hat{h}$  are fixed measurable functions. Define the test score

$$S := \frac{|Y - \hat{m}(X)|}{\hat{h}(X)}.$$

By exchangeability and the split nature of calibration, the scores  $\{S_i\}_{(X_i, Y_i) \in \mathcal{D}_{\text{cal}}}$  together with  $S$  are exchangeable conditional on  $\mathcal{D}_{\text{train}}$ . With  $\hat{q}$  chosen as the  $[(n_{\text{cal}} + 1)(1 - \alpha)]$ -th smallest calibration score, the standard split-conformal rank argument yields

$$\mathbb{P}(S \leq \hat{q} \mid \mathcal{D}_{\text{train}}) \geq 1 - \alpha.$$

Finally,  $S \leq \hat{q}$  is equivalent to  $|Y - \hat{m}(X)| \leq \hat{q} \hat{h}(X)$ , i.e.,  $Y \in \hat{C}(X)$ . Taking expectation over  $\mathcal{D}_{\text{train}}$  completes the proof.  $\square$

### A.4 Auxiliary lemmas

**Lemma 3** (Lipschitzness of  $\psi_x$ ). *Fix  $x$ . For any  $c, c' \in \mathbb{R}$ ,*

$$|\psi_x(c) - \psi_x(c')| \leq |c - c'|.$$

*Proof.* Let  $U = |Y - c| \mid X = x$  and  $V = |Y - c'| \mid X = x$ . By the reverse triangle inequality,  $|U - V| \leq |c - c'|$  almost surely. Hence  $U \leq V + |c - c'|$  and  $V \leq U + |c - c'|$  almost surely, implying  $Q_{1-\alpha}(U) \leq Q_{1-\alpha}(V) + |c - c'|$  and the reverse inequality by symmetry.  $\square$

**Lemma 4** (Coverage is Lipschitz in radius). *Under Assumption 2, for any fixed  $x$ , center  $c$ , and radii  $r_1, r_2 \geq 0$ ,*

$$\left| \mathbb{P}(|Y - c| \leq r_1 \mid X = x) - \mathbb{P}(|Y - c| \leq r_2 \mid X = x) \right| \leq 2f_{\max} |r_1 - r_2|.$$

*Proof.* Write  $\mathbb{P}(|Y - c| \leq r \mid X = x) = F_x(c + r) - F_x(c - r)$ , where  $F_x$  is the conditional CDF. By the mean value theorem and  $\sup f_x \leq f_{\max}$ ,  $|F_x(c + r_1) - F_x(c + r_2)| \leq f_{\max} |r_1 - r_2|$ , and similarly for the lower endpoint. Summing yields the bound.  $\square$

### A.5 Vanishing $\beta$ -bias of the $\beta$ -soft oracle

This section proves Lemma 2. Fix  $x$ . For any  $c \in \mathbb{R}$ , denote the endpoint imbalance map

$$G_x(c) := f_x(c + \psi_x(c)) - f_x(c - \psi_x(c)).$$

Also define the  $\beta$ -soft stationarity map

$$D_{x,\beta}(c) := \frac{\partial}{\partial c} \Phi_{x,\beta}(c, \psi_x(c)).$$

By Definition 1, any  $\beta$ -soft oracle center  $m_\beta(x)$  satisfies  $D_{x,\beta}(m_\beta(x)) = 0$ .

**Lemma 5** (Uniform lower bound on best-response radii). *Assume  $\sup_{x,y} f_x(y) \leq f_{\max}$ . Then for all  $x \in \mathcal{X}$  and all  $c \in \mathbb{R}$ ,*

$$\psi_x(c) \geq r_{\min} := \frac{1 - \alpha}{2f_{\max}}.$$

*In particular, any  $\beta$ -soft oracle radius  $h_\beta(x) = \psi_x(m_\beta(x))$  satisfies  $h_\beta(x) \geq r_{\min}$ .*

*Proof.* For any  $r \geq 0$ ,

$$\mathbb{P}(|Y - c| \leq r \mid X = x) = \int_{c-r}^{c+r} f_x(y) dy \leq 2r f_{\max}.$$

If  $r < (1 - \alpha)/(2f_{\max})$ , the right-hand side is strictly smaller than  $1 - \alpha$ , hence such an  $r$  cannot satisfy the feasibility constraint in the definition of  $\psi_x(c)$ .  $\square$

**Lemma 6** (Uniform kernel-smoothing consistency). *Fix  $x$  and recall  $f_{x,\beta} = f_x * K_\beta$ , where  $K_\beta(u) = \beta^{-1}\sigma'(u/\beta)$ . Under Assumptions 2 and 3,*

$$\sup_{z \in \mathbb{R}} |f_{x,\beta}(z) - f_x(z)| \rightarrow 0 \quad \text{as } \beta \rightarrow 0^+.$$

*Proof.* By Assumption 3,  $f_x$  is monotone on each tail, hence the limits  $\lim_{y \rightarrow \infty} f_x(y)$  and  $\lim_{y \rightarrow -\infty} f_x(y)$  exist. Since  $f_x$  is a density, these limits must be 0. Therefore  $f_x$  is continuous on  $\mathbb{R}$  and has finite limits at  $\pm\infty$ , which implies that  $f_x$  is uniformly continuous on  $\mathbb{R}$ .

Fix  $\varepsilon > 0$ . By uniform continuity, choose  $\delta > 0$  such that  $|f_x(z - u) - f_x(z)| \leq \varepsilon$  whenever  $|u| \leq \delta$ , uniformly in  $z$ . Then for all  $z$ ,

$$\begin{aligned} |f_{x,\beta}(z) - f_x(z)| &= \left| \int_{\mathbb{R}} (f_x(z - u) - f_x(z)) K_\beta(u) du \right| \\ &\leq \int_{|u| \leq \delta} \varepsilon K_\beta(u) du + \int_{|u| > \delta} 2f_{\max} K_\beta(u) du \\ &\leq \varepsilon + 2f_{\max} \int_{|u| > \delta} K_\beta(u) du \\ &= \varepsilon + 2f_{\max} \int_{|t| > \delta/\beta} \sigma'(t) dt. \end{aligned}$$

Since  $\sigma'$  is integrable,  $\int_{|t| > \delta/\beta} \sigma'(t) dt \rightarrow 0$  as  $\beta \rightarrow 0^+$ . Taking the supremum over  $z$  yields the claim.  $\square$

**Lemma 7** (Uniqueness of balance point). *Under Assumptions 2 and 3, the equation  $G_x(c) = 0$  has the unique solution  $c = m^*(x)$ . Moreover, for every  $\varepsilon > 0$  there exists  $\gamma_x(\varepsilon) > 0$  such that*

$$\inf_{|c - m^*(x)| \geq \varepsilon} |G_x(c)| \geq \gamma_x(\varepsilon).$$

*Proof.* Let  $c \in \mathbb{R}$  and set  $\ell = c - \psi_x(c)$ ,  $u = c + \psi_x(c)$ . By the definition of  $\psi_x(c)$  and the continuity of  $f_x$ , the constraint binds:  $\int_\ell^u f_x(y) dy = 1 - \alpha$ . If  $G_x(c) = 0$ , then  $f_x(u) = f_x(\ell) =: t$ . By unimodality,  $f_x(y) \geq t$  for all  $y \in [\ell, u]$ . Therefore  $[\ell, u]$  is a highest-density level set interval with mass  $1 - \alpha$ , indicating that it must coincide with the unique  $(1 - \alpha)$ -HDI, hence  $c = m^*(x)$ .

By Lemma 3,  $\psi_x(c)$  is continuous, and  $f_x$  is continuous, so  $G_x(c)$  is continuous. Moreover, as  $c \rightarrow \infty$ , we have  $u \rightarrow \infty$  and thus  $f_x(u) \rightarrow 0$ ; while  $\ell$  remains in a fixed lower tail quantile region, implying  $\limsup_{c \rightarrow \infty} G_x(c) < 0$ . Similarly,  $\liminf_{c \rightarrow -\infty} G_x(c) > 0$ . Hence there exists  $M < \infty$  such that  $\inf_{|c| \geq M} |G_x(c)| > 0$ .

Now fix  $\varepsilon > 0$ . On the compact set  $\{c : \varepsilon \leq |c - m^*(x)| \leq M\}$ , the continuous function  $|G_x(c)|$  attains its minimum, and the minimum is strictly positive by uniqueness of the root. Combining with the  $|c| \geq M$  region yields the stated  $\gamma_x(\varepsilon) > 0$ .  $\square$

**Proof of Lemma 2.**

*Proof.* Fix  $x$  and let  $m_\beta = m_\beta(x)$ ,  $h_\beta = h_\beta(x) = \psi_x(m_\beta)$ . By Lemma 1 applied with  $c$  and  $r = \psi_x(c)$ , for every  $c \in \mathbb{R}$ ,

$$D_{x,\beta}(c) = f_{x,\beta}(c + \psi_x(c)) - f_{x,\beta}(c - \psi_x(c)) + \varepsilon_{x,\beta}(c, \psi_x(c)),$$

$$|\varepsilon_{x,\beta}(c, \psi_x(c))| \leq 2f_{\max} \left( 1 - \sigma \left( \frac{\psi_x(c)}{\beta} \right) \right).$$

By Lemma 5,  $\psi_x(c) \geq r_{\min}$  for all  $c$ , hence

$$\sup_{c \in \mathbb{R}} |\varepsilon_{x,\beta}(c, \psi_x(c))| \leq 2f_{\max} \left( 1 - \sigma \left( \frac{r_{\min}}{\beta} \right) \right) \rightarrow 0 \quad \text{as } \beta \rightarrow 0^+.$$

Therefore, for all  $c$ ,

$$|D_{x,\beta}(c) - G_x(c)| \leq 2 \sup_{z \in \mathbb{R}} |f_{x,\beta}(z) - f_x(z)| + \sup_{c \in \mathbb{R}} |\varepsilon_{x,\beta}(c, \psi_x(c))|.$$

By Lemma 6, the right-hand side goes to 0, so

$$\sup_{c \in \mathbb{R}} |D_{x,\beta}(c) - G_x(c)| \rightarrow 0 \quad \text{as } \beta \rightarrow 0^+.$$

Note that  $D_{x,\beta}(m_\beta) = 0$  by Definition 1, then

$$|G_x(m_\beta)| = |G_x(m_\beta) - D_{x,\beta}(m_\beta)| \leq \sup_{c \in \mathbb{R}} |D_{x,\beta}(c) - G_x(c)| \rightarrow 0 \quad \text{as } \beta \rightarrow 0^+.$$

By Lemma 7, the root of  $G_x$  is isolated at  $m^*(x)$ , hence  $m_\beta \rightarrow m^*(x)$  as  $\beta \rightarrow 0^+$ .  $\square$

## A.6 Proof of Theorem 2

*Proof.* We prove (i)–(iii) and the decomposition (26).

**Length decomposition.** Recall  $|\widehat{C}(x)| = 2\widehat{q}\widehat{h}(x)$  and  $|C^*(x)| = 2h^*(x) = 2\psi_x(m^*(x))$ . Then

$$\begin{aligned} & \frac{1}{2} \left| |\widehat{C}(x)| - |C^*(x)| \right| \\ &= \left| \widehat{q}\widehat{h}(x) - \psi_x(m^*(x)) \right| \\ &\leq \left| \widehat{q}\widehat{h}(x) - \psi_x(m_{\beta_n}(x)) \right| + \left| \psi_x(m_{\beta_n}(x)) - \psi_x(m^*(x)) \right| \\ &\leq \left| \widehat{q} - 1 \right| \widehat{h}(x) + \left| \widehat{h}(x) - \psi_x(\widehat{m}(x)) \right| + \left| \psi_x(\widehat{m}(x)) - \psi_x(m_{\beta_n}(x)) \right| + \left| \psi_x(m_{\beta_n}(x)) - \psi_x(m^*(x)) \right| \\ &\leq \left| \widehat{q} - 1 \right| \widehat{h}(x) + \left| \widehat{h}(x) - \psi_x(\widehat{m}(x)) \right| + \left| \widehat{m}(x) - m_{\beta_n}(x) \right| + \left| m_{\beta_n}(x) - m^*(x) \right| \quad (\text{by Lemma 3}). \end{aligned}$$

Multiplying by 2 yields (26).

**Calibration factor  $\widehat{q} \rightarrow 1$ .** Define the (conditional-on-training) score CDF

$$F(t) := \mathbb{P}(S \leq t \mid \mathcal{D}_{\text{train}}), \quad S := \frac{|Y - \widehat{m}(X)|}{\widehat{h}(X)}$$

for a fresh  $(X, Y)$ . Let  $q := Q_{1-\alpha}(S \mid \mathcal{D}_{\text{train}})$ . We bound  $|\widehat{q} - 1| \leq |\widehat{q} - q| + |q - 1|$ .

(a) *Empirical quantile concentration.* Conditional on  $\mathcal{D}_{\text{train}}$ , the calibration scores are i.i.d. from  $F$ . By the DKW inequality, with probability at least  $1 - \delta$ ,

$$\sup_t |F_{n_{\text{cal}}}(t) - F(t)| \leq \varepsilon_{\text{DKW}} := \sqrt{\frac{1}{2n_{\text{cal}}} \log \frac{2}{\delta}}.$$

Let  $E_n := \{q \in (1 - \delta_0, 1 + \delta_0)\}$ . On the event  $E_n$ , Assumption 5 implies that  $F$  has a density bounded below by  $s_0$  on  $(1 - \delta_0, 1 + \delta_0)$ , so  $F$  is strictly increasing there and its inverse (quantile map) is locally Lipschitz with constant  $1/s_0$ . Therefore, on  $E_n$ ,  $|\hat{q} - q| \leq \varepsilon_{\text{DKW}}/s_0$ , yielding

$$|\hat{q} - q| = O_{\mathbb{P}} \left( \sqrt{\frac{\log n_{\text{cal}}}{n_{\text{cal}}}} \right),$$

where we will show in (b) that  $\mathbb{P}(E_n) \rightarrow 1$ .

(b) *The population score quantile  $q$  is close to 1.* Note that for each fixed  $x$ , by definition of  $\psi_x(\hat{m}(x))$  (continuity from Assumption 2),

$$\mathbb{P}(|Y - \hat{m}(x)| \leq \psi_x(\hat{m}(x)) \mid X = x) = 1 - \alpha.$$

Hence

$$|F(1) - (1 - \alpha)| = \left| \mathbb{E}[\mathbb{P}(|Y - \hat{m}(X)| \leq \hat{h}(X) \mid X) - \mathbb{P}(|Y - \hat{m}(X)| \leq \psi_X(\hat{m}(X)) \mid X) \mid \mathcal{D}_{\text{train}}] \right|.$$

By Lemma 4, the integrand is bounded by  $2f_{\max}|\hat{h}(X) - \psi_X(\hat{m}(X))|$ . Applying Cauchy–Schwarz and Assumption 6 yields

$$|F(1) - (1 - \alpha)| \leq 2f_{\max}\sqrt{\eta_{h,n}}$$

with probability at least  $1 - \rho_{h,n}$ . By Assumption 5,  $F$  has density at least  $s_0$  on  $(1 - \delta_0, 1 + \delta_0)$ ; for  $n$  large enough, the above bound implies  $q \in (1 - \delta_0, 1 + \delta_0)$ . Thus  $\mathbb{P}(E_n) \geq 1 - \rho_{h,n} \rightarrow 1$ , so the bound in (a) holds with probability tending to one, and then

$$|q - 1| \leq \frac{|F(1) - (1 - \alpha)|}{s_0} \leq \frac{2f_{\max}}{s_0}\sqrt{\eta_{h,n}}.$$

Combining (a)–(b) proves (i).

**Asymptotic conditional coverage.** For any fixed  $x$ ,

$$\begin{aligned} & \left| \mathbb{P}(Y \in \hat{C}(x) \mid X = x) - (1 - \alpha) \right| \\ &= \left| \mathbb{P}(|Y - \hat{m}(x)| \leq \hat{q}\hat{h}(x) \mid X = x) - \mathbb{P}(|Y - \hat{m}(x)| \leq \psi_x(\hat{m}(x)) \mid X = x) \right| \\ &\leq 2f_{\max} \left| \hat{q}\hat{h}(x) - \psi_x(\hat{m}(x)) \right| \quad (\text{by Lemma 4}) \\ &\leq 2f_{\max} \left( |\hat{q} - 1|\hat{h}(x) + |\hat{h}(x) - \psi_x(\hat{m}(x))| \right). \end{aligned}$$

Define

$$\Lambda_n := \left\{ x : |\hat{q} - 1| \leq \delta_n, |\hat{h}(x) - \psi_x(\hat{m}(x))| \leq \delta_n, \hat{h}(x) \leq h_{\max} \right\},$$

where  $\delta_n \rightarrow 0^+$  satisfies  $\delta_n \gg \sqrt{\eta_{h,n}} + \sqrt{\log n_{\text{cal}}/n_{\text{cal}}}$ . By (i) and Assumption 6,  $\mathbb{P}(X \in \Lambda_n) \rightarrow 1$ . On  $\Lambda_n$ , the conditional coverage error is at most  $2f_{\max}(h_{\max} + 1)\delta_n \rightarrow 0$ , which proves (ii).

**Oracle-efficient length.** Note the decomposition (26):

$$|\hat{C}(X)| - |C^*(X)| \leq 2|\hat{q} - 1|\hat{h}(X) + 2|\hat{h}(X) - \psi_X(\hat{m}(X))| + 2|\hat{m}(X) - m_{\beta_n}(X)| + 2|m_{\beta_n}(X) - m^*(X)|.$$

Combining (i), Assumptions 4 and 6, Lemma 2, and  $\beta_n \rightarrow 0^+$ , the right-hand side converges to 0 in probability, hence (iii) holds.  $\square$

## B Analysis of $\beta$ -bias Rates and Support Boundaries

This appendix complements Lemma 2 by providing (i) a second-order  $\beta$ -bias rate in the interior HDI regime under additional local smoothness assumptions, and (ii) an explicit first-order boundary shift when the oracle HDI is pinned at an active support boundary. We also explain why both cases are compatible with Theorem 2 without modifying its statement. Note that we work pointwise in  $x$  and suppress  $x$  to lighten notation in the following statement.

## B.1 Second-order $\beta$ -bias in the interior HDI regime

Let  $C^* = [\ell^*, u^*]$  be the unique interior  $(1 - \alpha)$ -HDI with  $m^* = (\ell^* + u^*)/2$  and  $h^* = (u^* - \ell^*)/2$ .

**Assumption 7** (Local  $C^2$  smoothness and non-flat HDI endpoints). There exists  $\delta > 0$  such that  $f$  is twice continuously differentiable on

$$[\ell^* - \delta, \ell^* + \delta] \cup [u^* - \delta, u^* + \delta], \quad \sup |f''| \leq M < \infty \text{ on this set.}$$

Moreover, the endpoint slopes are non-flat:

$$f'(\ell^*) > 0, \quad f'(u^*) < 0.$$

**Lemma 8** (Local logistic smoothing error). *Under Assumption 7, there exists a constant  $C < \infty$  such that for all sufficiently small  $\beta > 0$ ,*

$$\sup_{z \in [\ell^* - \delta/2, \ell^* + \delta/2]} |f_\beta(z) - f(z)| \leq C\beta^2, \quad \sup_{z \in [u^* - \delta/2, u^* + \delta/2]} |f_\beta(z) - f(z)| \leq C\beta^2,$$

where  $f_\beta = f * K_\beta$  and  $K_\beta(u) = \beta^{-1}\sigma'(u/\beta)$ .

*Proof.* Fix  $z$  in  $[\ell^* - \delta/2, \ell^* + \delta/2]$ . Write

$$f_\beta(z) - f(z) = \int_{\mathbb{R}} (f(z - u) - f(z)) K_\beta(u) du.$$

Split the integral into  $|u| \leq \delta/2$  and  $|u| > \delta/2$ .

On  $|u| \leq \delta/2$ , we have  $z - u \in [\ell^* - \delta, \ell^* + \delta]$  so Taylor's theorem yields

$$f(z - u) = f(z) - uf'(z) + \frac{u^2}{2} f''(\xi_{z,u})$$

for some  $\xi_{z,u}$  between  $z$  and  $z - u$ . Since  $K_\beta$  is symmetric,  $\int u K_\beta(u) du = 0$ , hence

$$\left| \int_{|u| \leq \delta/2} (f(z - u) - f(z)) K_\beta(u) du \right| \leq \frac{1}{2} \sup |f''| \int u^2 K_\beta(u) du = O(\beta^2),$$

because  $\int u^2 K_\beta(u) du = \beta^2 \int t^2 \sigma'(t) dt < \infty$ .

On  $|u| > \delta/2$ , we bound  $|f(z - u) - f(z)| \leq 2f_{\max}$  (boundedness) to get

$$\left| \int_{|u| > \delta/2} (f(z - u) - f(z)) K_\beta(u) du \right| \leq 2f_{\max} \int_{|u| > \delta/2} K_\beta(u) du = 2f_{\max} \int_{|t| > \delta/(2\beta)} \sigma'(t) dt,$$

which decays exponentially in  $1/\beta$  and in particular is  $o(\beta^2)$ . Combining both parts proves the claim. The argument around  $u^*$  is identical.  $\square$

**Proposition 2** (Second-order bias in interior case). *Assume the setting of Lemma 2 and, in addition, Assumption 7. Let  $m_\beta$  be any  $\beta$ -soft oracle center and  $h_\beta = \psi(m_\beta)$ . Then, as  $\beta \rightarrow 0^+$ ,*

$$|m_\beta - m^*| = O(\beta^2), \quad |h_\beta - h^*| = O(\beta^2).$$

*Proof.* By Lemma 2,  $m_\beta \rightarrow m^*$  and  $h_\beta \rightarrow h^*$ . Hence for sufficiently small  $\beta$ , the induced endpoints

$$\ell_\beta := m_\beta - h_\beta, \quad u_\beta := m_\beta + h_\beta$$

lie in the  $C^2$  neighborhoods of  $\ell^*$  and  $u^*$  in Assumption 7.

Soft stationarity and Lemma 1 imply

$$0 = \frac{\partial}{\partial c} \Phi_\beta(m_\beta, h_\beta) = f_\beta(u_\beta) - f_\beta(\ell_\beta) + \varepsilon_\beta, \quad |\varepsilon_\beta| \leq 2f_{\max}(1 - \sigma(h_\beta/\beta)).$$

By Lemma 5,  $h_\beta$  is uniformly bounded below away from 0, hence  $\varepsilon_\beta = o(\beta^2)$ .

Therefore,

$$|f(u_\beta) - f(\ell_\beta)| \leq |f(u_\beta) - f_\beta(u_\beta)| + |f(\ell_\beta) - f_\beta(\ell_\beta)| + |\varepsilon_\beta| = O(\beta^2)$$

by Lemma 8 (applied locally at  $\ell_\beta, u_\beta$ ).

Finally, we relate the density-imbalance  $G(c) := f(c + \psi(c)) - f(c - \psi(c))$  to the center error. By the definition of  $\psi(c)$ ,

$$\psi'(c) = -\frac{f(c + \psi(c)) - f(c - \psi(c))}{f(c + \psi(c)) + f(c - \psi(c))},$$

whenever  $f(c \pm \psi(c))$  exist and their sum is positive. In particular, we have  $G(m^*) = 0$ .

Under Assumption 7,  $f$  is  $C^2$  near  $\ell^*, u^*$ , hence  $G$  is  $C^1$  in a neighborhood of  $m^*$ . Differentiating  $G(c)$  and using  $\psi'(m^*) = 0$  gives

$$G'(m^*) = f'(u^*) - f'(\ell^*).$$

By Assumption 7,  $f'(\ell^*) > 0$  and  $f'(u^*) < 0$ , so  $G'(m^*) \neq 0$ . Therefore  $m^*$  is a simple root of  $G$ , and by the mean value theorem there exist  $m > 0$  and a neighborhood  $\mathcal{N}$  of  $m^*$  such that

$$|G(c)| \geq m|c - m^*|, \quad \forall c \in \mathcal{N}.$$

Applying this at  $c = m_\beta$  yields  $|m_\beta - m^*| = O(\beta^2)$ .

The radius bound follows from Lemma 3:

$$|h_\beta - h^*| = |\psi(m_\beta) - \psi(m^*)| \leq |m_\beta - m^*| = O(\beta^2).$$

□

## B.2 Active support boundaries: first-order $\beta$ shift

**Assumption 8** (Active lower-boundary truncation). Fix  $x$ . The conditional density  $f$  has support  $[a, b]$ , where  $b \in (a, \infty]$ . On  $(a, b)$ ,  $f$  is continuous, bounded by  $f_{\max}$ , and unimodal. We extend  $f(y) = 0$  for  $y \notin [a, b]$ , and assume the right limit  $f(a^+) := \lim_{y \rightarrow a^+} f(y)$  exists with  $0 < f(a^+) < \infty$ . The unique  $(1 - \alpha)$ -HDI is boundary-pinned:

$$C^* = [\ell^*, u^*] = [a, u^*], \quad u^*(x) \in (a, b),$$

and the boundary is *active* in the sense that  $f(a^+) > f(u^*)$ .

**Proposition 3** (First-order bias in an active support boundary). Fix  $x$  and suppose Assumption 8 holds. Let  $(m_\beta, h_\beta)$  be any  $\beta$ -soft oracle pair in Definition 1, and define endpoints

$$\ell_\beta := m_\beta - h_\beta, \quad u_\beta := m_\beta + h_\beta.$$

Let  $C^* = [a, u^*]$ , and define

$$\kappa := \log\left(\frac{f(u^*)}{f(a^+) - f(u^*)}\right), \quad \text{equivalently} \quad \sigma(\kappa) = \frac{f(u^*)}{f(a^+)}.$$

Then, as  $\beta \rightarrow 0^+$ ,

$$\ell_\beta = a + \kappa\beta + o(\beta), \quad \text{and} \quad ||C_\beta^*| - |C^*|| = O(\beta).$$

In particular,  $m_\beta \rightarrow m^*$  and  $h_\beta \rightarrow h^*$  as  $\beta \rightarrow 0^+$ .

*Proof.* Extend  $f(y) = 0$  for  $y \notin [a, b]$ . Recall  $f_\beta := f * K_\beta$ , where  $K_\beta(u) = \beta^{-1}\sigma'(u/\beta)$ . Let  $(c_\beta, r_\beta) := (m_\beta, h_\beta)$  be a  $\beta$ -soft oracle pair in Definition 1, and define endpoints

$$\ell_\beta := c_\beta - r_\beta, \quad u_\beta := c_\beta + r_\beta.$$

By definition,  $r_\beta = \psi_x(c_\beta)$ , so by continuity the feasibility constraint binds:

$$\int_{\ell_\beta}^{u_\beta} f(y) dy = 1 - \alpha. \tag{B.1}$$

We next organize the proof into five steps.

**1. Approximately balanced smoothed endpoints.** Lemma 1 gives

$$0 = \frac{\partial}{\partial c} \Phi_{x,\beta}(c_\beta, r_\beta) = f_\beta(u_\beta) - f_\beta(\ell_\beta) + \varepsilon_{x,\beta}(c_\beta, r_\beta), \quad |\varepsilon_{x,\beta}(c_\beta, r_\beta)| \leq 2f_{\max}(1 - \sigma(r_\beta/\beta)).$$

By Lemma 5,  $r_\beta \geq r_{\min} = (1 - \alpha)/(2f_{\max})$ , hence

$$f_\beta(u_\beta) - f_\beta(\ell_\beta) = O(1 - \sigma(r_{\min}/\beta)) = o(\beta), \quad \beta \rightarrow 0^+. \quad (\text{B.2})$$

**2. Prove  $\ell_\beta \rightarrow a$  and  $u_\beta \rightarrow u^*$ .** Suppose by contradiction that  $\ell_\beta \not\rightarrow a$ . Then there exist  $\delta > 0$  and a sequence  $\beta_k \rightarrow 0^+$  such that  $|\ell_{\beta_k} - a| \geq \delta$  for all  $k$ . We consider two cases.

*Case 1:  $\ell_{\beta_k} \leq a - \delta$  for all  $k$  along a subsequence.* Since  $f(y) = 0$  for  $y < a$ , the constraint (B.1) reduces to

$$\int_a^{u_{\beta_k}} f(y) dy = 1 - \alpha,$$

hence by uniqueness of  $u^*$  we have  $u_{\beta_k} = u^*$  for all  $k$  in this subsequence. Moreover, because  $\ell_{\beta_k} \leq a - \delta$ , we have  $f_{\beta_k}(\ell_{\beta_k}) \rightarrow 0$  as  $k \rightarrow \infty$ . Since  $u^* \in (a, b)$  is an interior point, smoothing disappears at  $u^*$  and  $f_{\beta_k}(u_{\beta_k}) = f_{\beta_k}(u^*) \rightarrow f(u^*)$ . As  $u^*$  lies in the support interior,  $f(u^*) > 0$ , hence

$$f_{\beta_k}(u_{\beta_k}) - f_{\beta_k}(\ell_{\beta_k}) \rightarrow f(u^*) > 0,$$

contradicting (B.2). Therefore Case 1 is impossible.

*Case 2:  $\ell_{\beta_k} \geq a + \delta$  for all  $k$  along a subsequence.* Then (B.1) implies  $F(\ell_{\beta_k}) \leq \alpha$ , so  $\ell_{\beta_k} \leq F^{-1}(\alpha)$  and  $\{\ell_{\beta_k}\}$  is bounded. We next show  $\{u_{\beta_k}\}$  is bounded as well. If not, then (passing to a further subsequence)  $u_{\beta_k} \rightarrow \infty$  (only possible when  $b = +\infty$ ). By unimodality,  $f(y) \rightarrow 0$  as  $y \rightarrow \infty$ , and consequently  $f_{\beta_k}(u_{\beta_k}) \rightarrow 0$ . On the other hand, since  $\ell_{\beta_k} \in [a + \delta, F^{-1}(\alpha)]$ , we may pass to a subsequence such that  $\ell_{\beta_k} \rightarrow \ell_0 \in [a + \delta, F^{-1}(\alpha)] \subset (a, b)$ . Because  $\ell_0$  is an interior point,  $f_{\beta_k}(\ell_{\beta_k}) \rightarrow f(\ell_0)$ , and as  $\ell_0 \in (a, b)$ , we have  $f(\ell_0) > 0$ . Hence

$$f_{\beta_k}(u_{\beta_k}) - f_{\beta_k}(\ell_{\beta_k}) \rightarrow -f(\ell_0) < 0,$$

again contradicting (B.2). Therefore  $\{u_{\beta_k}\}$  must be bounded.

Thus  $(\ell_{\beta_k}, u_{\beta_k})$  is bounded, and passing to a subsequence (not relabeled),  $(\ell_{\beta_k}, u_{\beta_k}) \rightarrow (\ell_0, u_0)$  with  $a + \delta \leq \ell_0 < u_0 < b$ . Then  $f_{\beta_k}(\ell_{\beta_k}) \rightarrow f(\ell_0)$  and  $f_{\beta_k}(u_{\beta_k}) \rightarrow f(u_0)$ . Letting  $k \rightarrow \infty$  in (B.2) yields  $f(\ell_0) = f(u_0)$ . Moreover, letting  $k \rightarrow \infty$  in (B.1) yields  $\int_{\ell_0}^{u_0} f = 1 - \alpha$ . This characterizes an interior  $(1 - \alpha)$ -HDI, contradicting Assumption 8 that the unique  $(1 - \alpha)$ -HDI is boundary-pinned at  $a$ .

Since both cases lead to contradictions, we conclude  $\ell_\beta \rightarrow a$ . Finally, (B.1) and  $\ell_\beta \rightarrow a$  imply  $u_\beta \rightarrow u^*$ , where  $u^*$  is the unique point satisfying  $\int_a^{u^*} f = 1 - \alpha$  (equivalently  $F(u^*) = 1 - \alpha$ ).

**3. Boundary scaling of the smoothed density.** Fix  $t \in \mathbb{R}$ . For  $y = a + \beta t$ ,

$$\begin{aligned} f_\beta(a + \beta t) &= \int_a^b f(z) \frac{1}{\beta} \sigma' \left( \frac{a + \beta t - z}{\beta} \right) dz \\ &= \int_0^{(b-a)/\beta} f(a + \beta w) \sigma'(t - w) dw \quad (\text{with } z = a + \beta w). \end{aligned}$$

Since  $f$  is bounded and  $\sigma'$  is integrable, dominated convergence yields

$$f_\beta(a + \beta t) \rightarrow f(a^+) \int_0^\infty \sigma'(t - w) dw = f(a^+) \sigma(t), \quad \beta \rightarrow 0^+. \quad (\text{B.3})$$

**4. Left endpoint expansion.** Define  $t_\beta := (\ell_\beta - a)/\beta$ . By Step 2,  $u_\beta \rightarrow u^* \in (a, b)$ , so  $f_\beta(u_\beta) \rightarrow f(u^*)$ . Then (B.2) implies  $f_\beta(\ell_\beta) \rightarrow f(u^*)$  as well. By Assumption 8,  $f(u^*)/f(a^+) \in (0, 1)$ , hence  $t_\beta$  must remain bounded (otherwise  $\sigma(t_\beta) \rightarrow 0$  or  $1$ , contradicting  $f_\beta(\ell_\beta) \rightarrow f(u^*)$ ). Taking limits in (B.3) along  $\ell_\beta = a + \beta t_\beta$  yields

$$f(a^+) \sigma(t_\beta) \rightarrow f(u^*), \quad \text{so} \quad \sigma(t_\beta) \rightarrow \frac{f(u^*)}{f(a^+)}.$$

Since  $\sigma$  is continuous and strictly increasing,  $t_\beta \rightarrow \kappa$ , where  $\sigma(\kappa) = f(u^*)/f(a^+)$ , i.e.,

$$\kappa = \log\left(\frac{f(u^*)}{f(a^+) - f(u^*)}\right).$$

Therefore  $\ell_\beta = a + \kappa\beta + o(\beta)$ .

**5. Right endpoint adaptation and length gap.** If  $\kappa = 0$ , then  $\ell_\beta = a + o(\beta)$ . Using (B.1) and  $\int_a^{u^*} f = 1 - \alpha$ , we obtain  $u_\beta = u^* + o(\beta)$ . Consequently

$$|C_\beta^*| - |C^*| = (u_\beta - \ell_\beta) - (u^* - a) = o(\beta).$$

If  $\kappa < 0$ , then  $\ell_\beta < a$  for all sufficiently small  $\beta$ . Because  $f(y) = 0$  for  $y < a$ , (B.1) reduces to  $\int_a^{u_\beta} f = 1 - \alpha$ , hence  $u_\beta = u^*$  by uniqueness. Thus  $|C_\beta^*| - |C^*| = (u^* - \ell_\beta) - (u^* - a) = -\kappa\beta + o(\beta)$ .

If  $\kappa > 0$ , then  $\ell_\beta > a$  for all sufficiently small  $\beta$ . Write  $u_\beta = u^* + \Delta_\beta$ . Using (B.1) and  $\int_a^{u^*} f = 1 - \alpha$ ,

$$0 = \int_{\ell_\beta}^{u_\beta} f - \int_a^{u^*} f = - \int_a^{\ell_\beta} f + \int_{u^*}^{u^* + \Delta_\beta} f.$$

By continuity at  $a^+$  and  $u^*$ , and  $\ell_\beta - a = \kappa\beta + o(\beta)$ , we have

$$\int_a^{\ell_\beta} f = (\ell_\beta - a) f(a^+) + o(\beta) = \kappa\beta f(a^+) + o(\beta), \quad \int_{u^*}^{u^* + \Delta_\beta} f = \Delta_\beta f(u^*) + o(\beta).$$

Hence  $\Delta_\beta = \kappa\beta f(a^+)/f(u^*) + o(\beta)$ , yielding the stated expansion for  $u_\beta$ . The length gap follows by direct subtraction:

$$|C_\beta^*| - |C^*| = (u_\beta - \ell_\beta) - (u^* - a) = \kappa\beta \left(\frac{f(a^+)}{f(u^*)} - 1\right) + o(\beta).$$

This completes the proof.  $\square$

*Remark 3* (Compatibility with Theorem 2). Proposition 3 implies  $|m_\beta(x) - m^*(x)| = O(\beta)$  in the boundary-pinned regime, hence the  $\beta_n$ -bias term in (26) still vanishes along any  $\beta_n \rightarrow 0^+$ . Therefore, the conclusions of Theorem 2 remain valid without modifying its statement.

## C Experimental Details

### C.1 Preprocessing

**Synthetic data.** Covariates are generated as  $X \sim \text{Unif}([-2, 2])$  and are used without further normalization. Targets are generated directly from the specified conditional distributions (Sec. 6.1).

**Real data.** On each run, we apply the following preprocessing steps *fit on the training split only*:

1. **Feature standardization:** we standardize each feature to zero mean and unit variance using the training split statistics, and apply the same transform to validation/calibration/test.
2. **Target stabilization:** for heavy-tailed targets, specifically, in *blog*, *facebook-1*, and *facebook-2*, we apply dataset-specific standard transformations commonly used in prior work (i.e.,  $\log(1 + y)$ ).
3. **Response rescaling:** we further rescale  $y$  by a constant  $c = \frac{1}{|\mathcal{D}_{\text{train}}|} \sum_{(x,y) \in \mathcal{D}_{\text{train}}} |y|$  computed on the training split, i.e.,  $y \leftarrow y/c$ . This improves numerical conditioning and does not affect coverage; it only rescales interval lengths by a constant shared across methods within each repetition.

## C.2 Neural architectures

**Backbone MLP (shared across methods).** All learning-based methods use the same backbone architecture: a two-hidden-layer MLP with 64 ReLU units per layer and a linear output layer. Method-specific heads enforce required constraints, e.g.:

- **Center of CoCP** outputs  $m(x) \in \mathbb{R}$ .
- **Radius of CoCP** outputs  $h(x) > 0$  by applying a Softplus nonlinearity.
- **CQR** outputs  $(\hat{q}_{\text{lo}}(x), \hat{q}_{\text{hi}}(x))$  via a base-and-gap parameterization to ensure monotonicity ( $\hat{q}_{\text{lo}} \leq \hat{q}_{\text{hi}}$ ).

## C.3 CoCP training details

**Cross-fitting and internal split.** CoCP trains a center  $m(x)$  and radius  $h(x)$  with  $K$ -fold cross-fitting. Within each repetition, CoCP uses  $K = 5$  folds on the training set. For each fold  $k$ , we use: (i) one fold as an internal validation set for early stopping, (ii) one fold for training the radius network  $h$ , and (iii) the remaining folds for training the center network  $m$ . This yields an effective 60%/20%/20% split within the cross-fitting pool for  $(m, h, \text{val})$ , respectively. Per fold, CoCP proceeds as: warmup  $m$ , alternating learning (repeat  $T = 5$  times), and final adjustment of  $h$ . The temperature parameter is set to  $\beta = 0.01$  in all experiments.

## C.4 Baseline implementation details

**Split.** We implement standard split conformal prediction with nonconformity score  $S(x, y) = |y - \hat{y}(x)|$ . The conformity threshold is computed on the calibration split using the standard finite-sample correction, and the resulting prediction interval is  $[\hat{y}(x) - \hat{q}, \hat{y}(x) + \hat{q}]$ .

**CQR.** We implement CQR following the standard split conformal recipe on top of a learned quantile model. The quantile network architecture matches the shared backbone (hidden 64, 2 layers, lr  $10^{-3}$ ). Conformal calibration is performed on the calibration split at the nominal coverage level.

**CHR.** For CHR, we employ an alternative faster implementation via CIR [19], using 98 interval components and the same MLP architecture as above (hidden 64, 2 layers, lr  $10^{-3}$ ).

**C-HDR.** We fit a conditional normalizing flow (CNF) model with 2 flow layers and MLP conditioners of width 64 (2 layers, learning rate  $2 \cdot 10^{-3}$ ). At test time, we approximate HDRs via Monte Carlo sampling using 5000 samples per test covariate. To ensure comparability with interval-based methods, we compute the convex hull of these samples to enforce a single connected prediction interval.

**CPCP.** We use the split fractions 0.4 and 0.4, and bandwidth  $\delta = 0.02$ . The underlying networks use the same MLP architecture with learning rate  $5 \cdot 10^{-4}$ . We enable clipping (`use_clip=true`, multiplier 5.0) and mixture augmentation (`use_mix=true`,  $\lambda_{\text{mix}} = 0.5$ ).

**RCP.** For RCP, we use the same MLP architecture to train the conditional quantile function of the nonconformity score on a fraction 0.5 of the calibration set (lr  $10^{-3}$ ), and we employ the same calibration step as CoCP via normalized score.

**CPL.** CPL relies on a user-specified finite-dimensional function class through a feature map  $\Phi(x)$ , used to define conditional moment constraints. We consider  $\Phi(x) = [1, x^T]^T$  in synthetic data and  $\Phi(x) = [1, \text{emb}(x)]^T$  in real data, where  $\text{emb}(x)$  is the embedding of  $x$  from the shared MLP model. We run 100 outer iterations. In each outer iteration, we train the threshold network  $h_\theta$  for 200 steps on real data (resp. 500 steps on 1D synthetic data), with learning rate  $10^{-3}$ , and we update the nonnegative multipliers with learning rate 0.2. We use smoothing parameter of 0.1, length penalty weight 1.0, and split ratio 0.7 for the internal CPL split.

**Naive CC.** The RKHS-based conditional conformal method of [17] can be extremely computationally expensive in our setting. We therefore include it *only* on synthetic data, and use a simplified variant that omits *test imputation*. Under i.i.d. sampling and large sample sizes, this “naive” variant is empirically close to the full method while being significantly more tractable. We do not run this baseline on real datasets. We use an RBF kernel

$$k_\gamma(x, x') = \exp(-\gamma\|x - x'\|_2^2),$$

with  $(\gamma = 0.5, \lambda = 0.00025)$  and a finite-dimensional feature map  $\Phi(x)$  as in CPL. In our implementation, the (nonnegative) interval radius is parameterized as

$$t(x) = \max\{0, K(x, X_{\text{cal}})w + \Phi(x)^\top \nu\},$$

where  $K(x, X_{\text{cal}})$  is the vector of kernel evaluations against the calibration covariates.

## C.5 Metrics and estimation

Let  $\hat{C}(x) = [\hat{\ell}(x), \hat{u}(x)]$  denote the predicted interval and define the empirical coverage indicator:

$$Z_i = \mathbb{1}\{y_i \in [\hat{\ell}(x_i), \hat{u}(x_i)]\}.$$

**Coverage and Length.** On both synthetic and real datasets, we report:

$$\text{Coverage} = \frac{1}{n_{\text{test}}} \sum_{i=1}^{n_{\text{test}}} Z_i, \quad \text{Length} = \frac{1}{n_{\text{test}}} \sum_{i=1}^{n_{\text{test}}} (\hat{u}(x_i) - \hat{\ell}(x_i)).$$

**ConMAE.** On synthetic datasets, the conditional distribution  $Y \mid X = x$  is known. For each test covariate  $x_i$ , we compute the *exact* conditional coverage of the predicted interval using the true conditional CDF  $F_{x_i}$ :

$$c_i = \mathbb{P}(Y \in \hat{C}(x_i) \mid X = x_i) = F_{x_i}(\hat{u}(x_i)) - F_{x_i}(\hat{\ell}(x_i)).$$

We then report the mean absolute deviation from the target  $1 - \alpha$ :

$$\text{ConMAE} = \frac{1}{n_{\text{test}}} \sum_{i=1}^{n_{\text{test}}} |c_i - (1 - \alpha)|.$$

**MSCE.** We estimate the MSCE using a partition-wise (histogram-style) estimator as in [4]. We run K-means on the standardized test covariates  $\{x_i\}$  to obtain  $K$  clusters  $\{\mathcal{G}_1, \dots, \mathcal{G}_K\}$  (we use  $K = 10$  throughout). For each cluster  $g$ , define the empirical coverage

$$\hat{c}_g = \frac{1}{|\mathcal{G}_g|} \sum_{i \in \mathcal{G}_g} Z_i.$$

We then compute the test-mass-weighted squared deviation from the target level  $1 - \alpha$ :

$$\widehat{\text{MSCE}} = \sum_{g=1}^K \frac{|\mathcal{G}_g|}{n_{\text{test}}} (\hat{c}_g - (1 - \alpha))^2.$$

This estimator highlights the usual bias–variance trade-off: larger  $K$  yields a finer approximation of conditional coverage, but reduces the number of samples per cluster, making  $\hat{c}_g$  noisier. Moreover, because K-means relies on Euclidean distances, the partition can become unreliable in high dimensions, so MSCE should be interpreted as a diagnostic rather than an exact estimate of conditional coverage.

**WSC.** We evaluate WSC following [7] and using the implementation provided in the `covmetrics` package [4]. Given a mass threshold  $\delta \in (0, 1]$  (we use  $\delta = 0.1$ ), WSC scans (a finite set of) slabs in the feature space and reports the *minimum* empirical coverage over all slabs whose empirical mass is at least  $\delta$ . Higher WSC indicates better worst-case conditional behavior; values substantially below  $1 - \alpha$  suggest localized undercoverage.

**ERT.** We compute ERT using the `covmetrics` package [4]. ERT casts conditional coverage evaluation as a classification problem: predict  $Z = \mathbb{1}\{Y \in \hat{C}(X)\}$  from  $X$ . Let  $h : \mathcal{X} \rightarrow [0, 1]$  be a probabilistic auditor and  $\ell$  a proper loss. ERT is defined as the excess risk over the constant baseline  $1 - \alpha$ :

$$\widehat{\ell\text{-ERT}} = \widehat{R}_\ell(1 - \alpha) - \widehat{R}_\ell(h), \quad \widehat{R}_\ell(h) = \frac{1}{n_{\text{test}}} \sum_{i=1}^{n_{\text{test}}} \ell(h(x_i), Z_i).$$

To avoid overfitting the auditor on the same data it is evaluated on, we follow [4] and estimate ERT with  $k$ -fold cross-fitting on the test set (as implemented in `covmetrics`). In all experiments, we instantiate the auditor as a Logistic Regression classifier and report  $\ell_1$ -ERT and  $\ell_2$ -ERT (Brier-score-based) returned by `covmetrics`. Due to finite-sample noise, ERT estimates can occasionally be slightly negative; such values should be interpreted as being statistically close to zero.

## D Additional Experimental Results

### D.1 Ablation study on alternating iterations

To investigate the convergence behavior and the necessity of the proposed alternating optimization mechanism, we ablate the number of iterations ( $T = 0, 1, \dots, 5$ ) on synthetic datasets, keeping  $K = 5$  folds cross-fitting and ensembling. Figure 7 visualizes the convergence trajectories, while Table 4 details the exact numerical performance. Here,  $T = 0$  represents an interval using only the MSE-pre-trained center without soft-coverage refinement.

The necessity of co-optimization depends heavily on data skewness. For the symmetric Normal distribution, the conditional mean already coincides with the true HDI center. Thus, the MSE-initialized center is near-optimal, and further updates yield only marginal improvements. Conversely, under skewness, the mean deviates from the HDI center, making alternating updates essential. On the LogNormal dataset, the process converges rapidly around  $T = 2$ , where the trade-off between interval length and conditional coverage error (ConMAE) effectively stabilizes.

This dynamic is most pronounced on the highly skewed Exponential dataset. At  $T = 0$ , the misaligned MSE center forces the radius to over-expand to capture the required mass, resulting in an inefficiently wide interval (Length 1.2293). As  $T$  increases, the soft-coverage objective actively translates the center toward higher-density regions, allowing the radius to contract. As shown by the steep descent in Figure 7, the length drops drastically to 1.1337 by  $T = 4$ , while maintaining a highly competitive ConMAE (0.0069). To ensure robust convergence across unknown distributions without dataset-specific tuning, we uniformly adopt  $T = 5$  as a safe default in our main experiments.

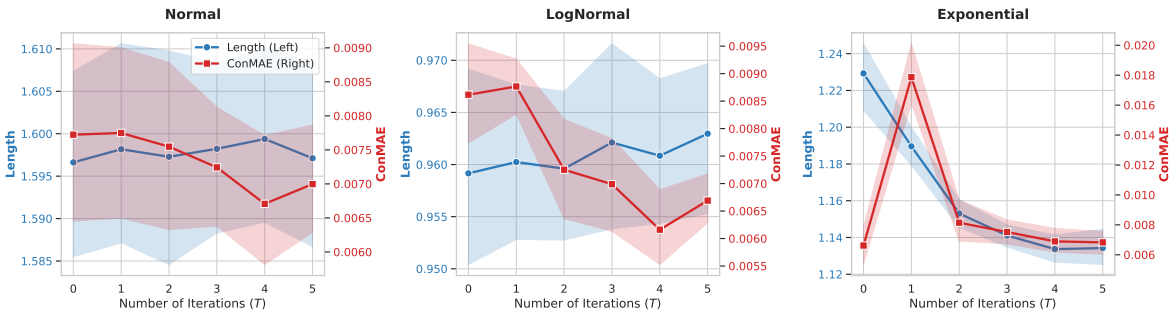


Figure 7: **Convergence dynamics of CoCP over alternating iterations ( $T$ ).** The plots visualize the trade-off between interval length (blue, left axis) and conditional coverage error (ConMAE; red, right axis). While symmetric distributions (Normal) are near-optimal at  $T = 0$ , skewed distributions require alternating updates to optimize this trade-off, achieving either significantly lower ConMAE (LogNormal) or drastically reduced interval length (Exponential).

Table 4: Ablation study on the number of alternating iterations ( $T$ ) on synthetic datasets, including  $T = 0$ . Results are averaged over 10 splits (mean  $\pm$  std). Training time is reported in seconds.

Dataset	$T$	Coverage	Length ( $\downarrow$ )	ConMAE ( $\downarrow$ )	Train Time (s)
Normal	0	0.9013 (0.0039)	1.5966 (0.0187)	0.0077 (0.0021)	14.71 (2.57)
	1	0.9014 (0.0043)	1.5982 (0.0206)	0.0077 (0.0022)	29.37 (3.52)
	2	0.9005 (0.0044)	1.5973 (0.0203)	0.0075 (0.0021)	42.64 (4.18)
	3	0.9007 (0.0041)	1.5982 (0.0170)	0.0072 (0.0015)	56.02 (5.34)
	4	0.9008 (0.0037)	1.5994 (0.0180)	0.0067 (0.0017)	69.49 (6.33)
	5	0.9003 (0.0041)	1.5971 (0.0187)	0.0070 (0.0014)	82.47 (7.57)
LogNormal	0	0.9009 (0.0034)	0.9592 (0.0161)	0.0086 (0.0015)	14.77 (2.33)
	1	0.9014 (0.0028)	0.9602 (0.0126)	0.0088 (0.0009)	30.58 (5.11)
	2	0.9005 (0.0031)	0.9596 (0.0128)	0.0073 (0.0016)	44.57 (6.20)
	3	0.9008 (0.0035)	0.9621 (0.0153)	0.0070 (0.0014)	58.07 (6.64)
	4	0.9006 (0.0027)	0.9608 (0.0117)	0.0062 (0.0011)	72.72 (7.89)
	5	0.9008 (0.0030)	0.9630 (0.0129)	0.0067 (0.0007)	86.72 (9.27)
Exponential	0	0.8970 (0.0031)	1.2293 (0.0318)	0.0066 (0.0021)	14.89 (2.18)
	1	0.8961 (0.0025)	1.1896 (0.0172)	0.0179 (0.0032)	50.68 (19.82)
	2	0.8965 (0.0030)	1.1530 (0.0130)	0.0081 (0.0024)	75.70 (27.15)
	3	0.8971 (0.0033)	1.1411 (0.0104)	0.0075 (0.0014)	100.76 (36.14)
	4	0.8969 (0.0027)	1.1337 (0.0127)	0.0069 (0.0014)	122.31 (42.26)
	5	0.8971 (0.0027)	1.1342 (0.0160)	0.0068 (0.0013)	146.25 (50.22)

## References

- [1] Anastasios N Angelopoulos and Stephen Bates. A gentle introduction to conformal prediction and distribution-free uncertainty quantification. *arXiv preprint arXiv:2107.07511*, 2021.
- [2] Konstantina Bairaktari, Jiayun Wu, and Steven Wu. Kandinsky conformal prediction: Beyond class- and covariate-conditional coverage. In *Forty-second International Conference on Machine Learning*, 2025. URL <https://openreview.net/forum?id=IHAnkPkoIX>.
- [3] Jie Bao, Nicolo Colombo, Valery Manokhin, Suqun Cao, and Rui Luo. A review and comparative analysis of univariate conformal regression methods. In Khuong An Nguyen, Zhiyuan Luo, Harris Papadopoulos, Tuwe L fstr m, Lars Carlsson, and Henrik Bostr m, editors, *Proceedings of the Fourteenth Symposium on Conformal and Probabilistic Prediction with Applications*, volume 266 of *Proceedings of Machine Learning Research*, pages 282–304. PMLR, 10–12 Sep 2025. URL <https://proceedings.mlr.press/v266/bao25a.html>.
- [4] Sacha Braun, David Holzm ller, Michael I. Jordan, and Francis Bach. Conditional coverage diagnostics for conformal prediction, 2025. URL <https://arxiv.org/abs/2512.11779>.
- [5] Krisztian Buza. BlogFeedback. UCI Machine Learning Repository, 2014. DOI: <https://doi.org/10.24432/C58S3F>.
- [6] George Casella and Roger Berger. *Statistical inference*. Chapman and Hall/CRC, 2024.
- [7] Maxime Cauchois, Suyash Gupta, and John C. Duchi. Knowing what you know: valid and validated confidence sets in multiclass and multilabel prediction. *J. Mach. Learn. Res.*, 22(1), January 2021. ISSN 1532-4435.
- [8] Qianyi Chen and Bo Li. Colorful pinball: Density-weighted quantile regression for conditional guarantee of conformal prediction, 2026. URL <https://arxiv.org/abs/2512.24139>.
- [9] Victor Chernozhukov, Kaspar W thrich, and Yinchu Zhu. Distributional conformal prediction. *Proceedings of the National Academy of Sciences*, 118(48):e2107794118, 2021.

- [10] Nicolo Colombo. On training locally adaptive cp. In Harris Papadopoulos, Khuong An Nguyen, Henrik Boström, and Lars Carlsson, editors, *Proceedings of the Twelfth Symposium on Conformal and Probabilistic Prediction with Applications*, volume 204 of *Proceedings of Machine Learning Research*, pages 384–398. PMLR, 13–15 Sep 2023.
- [11] Nicolas Deutschmann, Mattia Rigotti, and Maria Rodriguez Martinez. Adaptive conformal regression with split-jackknife+ scores. *Transactions on Machine Learning Research*, 2024. ISSN 2835-8856. URL <https://openreview.net/forum?id=1fbTGC3BUD>.
- [12] Victor Dheur, Matteo Fontana, Yorick Estievenart, Naomi Desobry, and Souhaib Ben Taieb. A unified comparative study with generalized conformity scores for multi-output conformal regression. In *Forty-second International Conference on Machine Learning*, 2025. URL <https://openreview.net/forum?id=G8R3niOMI4>.
- [13] Hadi Fanaee-T. Bike Sharing. UCI Machine Learning Repository, 2013. DOI: <https://doi.org/10.24432/C5W894>.
- [14] Rina Foygel Barber, Emmanuel J Candès, Aaditya Ramdas, and Ryan J Tibshirani. The limits of distribution-free conditional predictive inference. *Information and Inference: A Journal of the IMA*, 10(2):455–482, 08 2020. ISSN 2049-8772. doi: 10.1093/imaia/iaaa017.
- [15] Chao Gao, Liren Shan, Vaidehi Srinivas, and Aravindan Vijayaraghavan. Volume optimality in conformal prediction with structured prediction sets. In *Forty-second International Conference on Machine Learning*, 2025. URL <https://openreview.net/forum?id=oNDhnGrD51>.
- [16] Matteo Gasparin and Aaditya Ramdas. Improving the statistical efficiency of cross-conformal prediction. In *Forty-second International Conference on Machine Learning*, 2025. URL <https://openreview.net/forum?id=mxNEWzqXFH>.
- [17] Isaac Gibbs, John J Cherian, and Emmanuel J Candès. Conformal prediction with conditional guarantees. *Journal of the Royal Statistical Society Series B: Statistical Methodology*, 87(4):1100–1126, 03 2025. ISSN 1369-7412. doi: 10.1093/jrsssb/qkaf008.
- [18] Leying Guan. Localized conformal prediction: a generalized inference framework for conformal prediction. *Biometrika*, 110(1):33–50, 07 2022. ISSN 1464-3510. doi: 10.1093/biomet/asac040.
- [19] Naixin Guo, Rui Luo, and Zhixin Zhou. Fast conformal prediction using conditional interquartile intervals, 2026. URL <https://arxiv.org/abs/2601.02769>.
- [20] Kam Hamidieh. Superconductivity Data. UCI Machine Learning Repository, 2018. DOI: <https://doi.org/10.24432/C53P47>.
- [21] harlfoxem. House sales in king county, usa, 2016. URL <https://www.kaggle.com/datasets/harlfoxem/housesalesprediction>. Accessed: 2026-03-01.
- [22] Rohan Hore and Rina Foygel Barber. Conformal prediction with local weights: randomization enables robust guarantees. *Journal of the Royal Statistical Society Series B: Statistical Methodology*, 87(2):549–578, 11 2024. ISSN 1369-7412. doi: 10.1093/jrsssb/qkae103.
- [23] Rob J. Hyndman. Computing and graphing highest density regions. *The American Statistician*, 50(2):120–126, 1996. ISSN 00031305. URL <http://www.jstor.org/stable/2684423>.
- [24] Rafael Izbicki, Gilson Shimizu, and Rafael B Stern. Cd-split and hpd-split: Efficient conformal regions in high dimensions. *Journal of Machine Learning Research*, 23(87):1–32, 2022.
- [25] Yeo Jin Jung, Yating Liu, Zixuan Wu, So Won Jeong, and Claire Donnat. Speedcp: Fast kernel-based conditional conformal prediction, 2025. URL <https://arxiv.org/abs/2509.24100>.
- [26] Shayan Kiyani, George Pappas, and Hamed Hassani. Conformal prediction with learned features. In *Proceedings of the 41st International Conference on Machine Learning*, ICML’24. JMLR.org, 2024.

- [27] Shayan Kiyani, George Pappas, and Hamed Hassani. Length optimization in conformal prediction. In *Proceedings of the 38th International Conference on Neural Information Processing Systems*, NIPS '24, Red Hook, NY, USA, 2024. Curran Associates Inc. ISBN 9798331314385.
- [28] Jing Lei and Larry Wasserman. Distribution-free prediction bands for non-parametric regression. *Journal of the Royal Statistical Society Series B: Statistical Methodology*, 76(1):71–96, 2014.
- [29] Jing Lei, Max G’Sell, Alessandro Rinaldo, Ryan J Tibshirani, and Larry Wasserman. Distribution-free predictive inference for regression. *Journal of the American Statistical Association*, 113(523): 1094–1111, 2018.
- [30] Rui Luo and Zhixin Zhou. Conformal thresholded intervals for efficient regression. In *Proceedings of the AAAI Conference on Artificial Intelligence*, volume 39, pages 19216–19223, 2025.
- [31] Harris Papadopoulos, Kostas Proedrou, Volodya Vovk, and Alex Gammerman. Inductive confidence machines for regression. In *European conference on machine learning*, pages 345–356. Springer, 2002.
- [32] Tim Pearce, Alexandra Brintrup, Mohamed Zaki, and Andy Neely. High-quality prediction intervals for deep learning: A distribution-free, ensembled approach. In Jennifer Dy and Andreas Krause, editors, *Proceedings of the 35th International Conference on Machine Learning*, volume 80 of *Proceedings of Machine Learning Research*, pages 4075–4084. PMLR, 10–15 Jul 2018. URL <https://proceedings.mlr.press/v80/pearce18a.html>.
- [33] Vincent Plassier, Alexander Fishkov, Victor Dheur, Mohsen Guizani, Souhaib Ben Taieb, Maxim Panov, and Eric Moulines. Rectifying conformity scores for better conditional coverage. In *Forty-second International Conference on Machine Learning*, 2025. URL <https://openreview.net/forum?id=STeHUnCmdm>.
- [34] Prashant Rana. Physicochemical Properties of Protein Tertiary Structure. UCI Machine Learning Repository, 2013. DOI: <https://doi.org/10.24432/C5QW3H>.
- [35] Yaniv Romano, Evan Patterson, and Emmanuel J. Candès. Conformalized quantile regression. In *Proceedings of the 33rd International Conference on Neural Information Processing Systems*, Red Hook, NY, USA, 2019. Curran Associates Inc.
- [36] Yaniv Romano, Matteo Sesia, and Emmanuel Candès. Classification with valid and adaptive coverage. *Advances in neural information processing systems*, 33:3581–3591, 2020.
- [37] Matteo Sesia and Emmanuel J Candès. A comparison of some conformal quantile regression methods. *Stat*, 9(1):e261, 2020.
- [38] Matteo Sesia and Yaniv Romano. Conformal prediction using conditional histograms. In A. Beygelzimer, Y. Dauphin, P. Liang, and J. Wortman Vaughan, editors, *Advances in Neural Information Processing Systems*, 2021. URL <https://openreview.net/forum?id=EvhsTX6GMym>.
- [39] Glenn Shafer and Vladimir Vovk. A tutorial on conformal prediction. *J. Mach. Learn. Res.*, 9: 371–421, June 2008. ISSN 1532-4435.
- [40] Kamaljot Singh. Facebook Comment Volume. UCI Machine Learning Repository, 2015. DOI: <https://doi.org/10.24432/C5Q886>.
- [41] Ryan J. Tibshirani, Rina Foygel Barber, Emmanuel J. Candès, and Aaditya Ramdas. *Conformal prediction under covariate shift*. Curran Associates Inc., Red Hook, NY, USA, 2019.
- [42] Vladimir Vovk. Cross-conformal predictors. *Annals of Mathematics and Artificial Intelligence*, 74 (1):9–28, 2015.
- [43] Vladimir Vovk, Alexander Gammerman, and Glenn Shafer. *Algorithmic learning in a random world*. Springer, 2005.